The Plant Cell, Vol. 32: 1749–1767, May 2020, www.plantcell.org © 2020 ASPB.

Biochemical and Genetic Analysis Identify CSLD3 as a beta-1,4-Glucan Synthase That Functions during Plant Cell Wall Synthesis[OPEN]

Jiyuan Yang,[a,1] Gwangbae Bak,[a,1] Tucker Burgin,[b] William J. Barnes,[c,d] Heather B. Mayes,[b] Maria J. Peña,[c] Breeanna R. Urbanowicz,[c,d] and Erik Nielsen[a,2]

[a] Department of Molecular, Cellular, and Developmental Biology, University of Michigan, Ann Arbor, Michigan 48109
[b] Department of Chemical Engineering, University of Michigan, Ann Arbor, Michigan 48109
[c] Complex Carbohydrate Research Center, University of Georgia, Athens, Georgia 30602
[d] Department of Biochemistry and Molecular Biology, University of Georgia, Athens, Georgia 30602

ORCID IDs: 0000-0003-0185-1133 (J.Y.); 0000-0002-4433-8391 (G.B.); 0000-0002-3714-3537 (T.B.); 0000-0003-3297-4136 (W.J.B.); 0000-0001-9373-0106 (H.B.M.); 0000-0002-1672-0067 (M.J.P.); 0000-0001-5247-4513 (B.U.); 0000-0003-3565-0073 (E.N.)

In plants, changes in cell size and shape during development fundamentally depend on the ability to synthesize and modify cell wall polysaccharides. The main classes of cell wall polysaccharides produced by terrestrial plants are cellulose, hemicelluloses, and pectins. Members of the cellulose synthase (CESA) and cellulose synthase-like (CSL) families encode glycosyltransferases that synthesize the β-1,4-linked glycan backbones of cellulose and most hemicellulosic polysaccharides that comprise plant cell walls. Cellulose microfibrils are the major load-bearing component in plant cell walls and are assembled from individual β-1,4-glucan polymers synthesized by CESA proteins that are organized into multimeric complexes called CESA complexes, in the plant plasma membrane. During distinct modes of polarized cell wall deposition, such as in the tip growth that occurs during the formation of root hairs and pollen tubes or de novo formation of cell plates during plant cytokinesis, newly synthesized cell wall polysaccharides are deposited in a restricted region of the cell. These processes require the activity of members of the CESA-like D subfamily. However, while these CSLD polysaccharide synthases are essential, the nature of the polysaccharides they synthesize has remained elusive. Here, we use a combination of genetic rescue experiments with CSLD-CESA chimeric proteins, in vitro biochemical reconstitution, and supporting computational modeling and simulation, to demonstrate that Arabidopsis (*Arabidopsis thaliana*) CSLD3 is a UDP-glucose-dependent β-1,4-glucan synthase that forms protein complexes displaying similar ultrastructural features to those formed by CESA6.

INTRODUCTION

Cellulose is one of the most abundant organic polymers in nature and is the principal component of the plant cell wall, providing most of its tensile strength (Baskin, 2005; Cosgrove, 2005). Cellulose microfibrils contain multiple β-1,4-glucan chains that associate via intermolecular hydrogen bonds and are synthesized by large, membrane-localized complexes called "rosette complexes" (Baskin, 2005; Cosgrove, 2005). In Arabidopsis (*Arabidopsis thaliana*), cellulose synthase (CESA) proteins interact to form rosette subunits, and six of these subunits then assemble into multimeric rosette complexes, often referred to as CESA complexes (CSCs; Kimura et al., 1999). CSCs contain several CESA subunits, each thought to be capable of synthesizing β-1,4-glucan polysaccharides. Arabidopsis contains 10 *CESA* genes, of which the proteins encoded by at least three, CESA1, CESA3, and CESA6 or CESA2/5/9, are required for cellulose synthesis during primary cell wall formation (Arioli et al., 1998; Fagard et al., 2000; Scheible and Pauly, 2004). While earlier models suggested each rosette subunit may contain six CESA proteins, recent studies combining ultrastructural analysis and computer-modeling of plant CESAs using bacterial CESA structures have proposed rosette subunits may contain as few as three CESAs each (Nixon et al., 2016; Vandavasi et al., 2016). Furthermore, in vitro reconstitution of CESA activity was observed in proteoliposomes containing only *Populus tremula x tremuloides* CESA8 (*Ptt*CESA8) or *Physcomitrella patens* CESA8 (*Pp*CESA8; Purushotham et al., 2016; Cho et al., 2017), highlighting that our understanding of the composition of functional CESA rosette complexes remains incomplete.

In addition to cellulose and pectin, primary cell walls of terrestrial plants also contain hemicellulosic polysaccharides, such as xyloglucan, β-1,4-xylans, and β-1,4-mannans (Baskin, 2005; Cosgrove, 2005). CESA proteins and members of the Cellulose Synthase-Like (CSL) family are classified as family 2 glycosyltransferases (GT2s) in the Carbohydrate-Active enZYmes Database (Lombard et al., 2014). In plants, members of this family that have been characterized synthesize the glycan backbones of cellulose and most hemicellulosic polysaccharides, with the exception of β-1,4-xylan (Scheible and Pauly, 2004; Liepman et al., 2010; Smith et al., 2017). Members of the CESA superfamily have been resolved into seven lineages in Arabidopsis, including the CESAs and six CSL clades:

[1] These authors contributed equally to this work.
[2] Address correspondence to nielsene@umich.edu.
The author(s) responsible for distribution of materials integral to the findings presented in this article in accordance with the policy described in the Instructions for Authors (www.plantcell.org) is: Erik Nielsen (nielsene@umich.edu).
[OPEN]Articles can be viewed without a subscription.
www.plantcell.org/cgi/doi/10.1105/tpc.19.00637

IN A NUTSHELL

Background: As the most abundant organic compound in the world, cellulose microfibrils provide strength and rigidity to the primary cell walls of land plants. It is generally accepted that cellulose is synthesized by large, multi-subunit, membrane-localized cellulose synthase complexes (CSCs), which contain at least three different isoforms of cellulose synthase (CESA) proteins. Each of these CESA proteins synthesizes individual beta-1,4-glucan polysaccharides, which then assemble into cellulose microfibrils. Recent studies have highlighted novel roles for a related class of cellulose synthase-like D (CSLD) proteins in certain types of polarized cell wall deposition. While several different biosynthetic activities have been proposed for CSLD proteins, the nature of the polysaccharides generated by CSLD proteins has remained controversial.

Question: We wanted to definitively establish the biosynthetic activity of one member of the CSLD protein family, CSLD3. To do this, we utilized a combination of biochemical purification and in vitro reconstitution, and genetic complementation methods.

Findings: We found that a chimeric fusion of a cellulose synthase component, CESA6, that contained the catalytic domain of CSLD3, genetically complemented both developmental and cell wall defects in *cesa6* mutant plants. These chimeric proteins assembled into functional cellulose synthase complexes, and the catalytic activity of the chimeric fusion proteins was required for these complexes to functionally rescue *cesa6* mutant cell wall defects. Furthermore, we demonstrated UDP-glucose dependent β-1,4-glucan synthase activities for purified CESA6 and CSLD3 proteins in vitro, and found that detergent-solubilized CESA6 and CSLD3 proteins assembled into complexes that looked similar to one another, and which displayed some structural similarities to subunits of plant cellulose synthase complexes observed using EM techniques in vivo.

Next steps: It is unclear whether all members of the CSLD protein family are beta-1,4-glucan synthases like CSLD3. In addition, while CESA6 and CSLD3 proteins assembled into similar sized complexes, in planta, these CESA protein complexes further assemble into higher-order cellulose synthase complexes. Whether this occurs for CSLD proteins as well is still unknown, as is the question of whether CSLD-synthesized beta-1,4-glycan polymers assemble into cellulose microfibrils, or some other form of beta-1,4-glucan cell wall polymer.

CSLA, CSLB, CSLC, CSLD, CSLE, and CSLG (Richmond and Somerville, 2000; Little et al., 2018). *CSLA*s were shown to encode proteins that synthesize β-1,4-mannans, catalyzing formation of β-1,4-mannan and glucomannan in vitro when heterologously expressed in insect cells (Dhugga et al., 2004; Liepman et al., 2005). At least one member of the *CSLC* family has been implicated in synthesis of the β-1,4-glucan backbone of xyloglucan in the Golgi apparatus (Cocuron et al., 2007), and other CSLCs have been localized to the plasma membrane, where they may synthesize noncrystalline β-1,4-glucan (Dwivany et al., 2009). Members of the *CSLF*, *CSLH*, and *CSLJ* families, which are largely present only in cereals and grasses, predominantly synthesize mixed-linkage (1,3;1,4)-β-glucans (Burton et al., 2006; Doblin et al., 2009; Little et al., 2018). Recently, two members of the *CSLF* family from *Hordeum vulgare* (*Hv*CSLF3 and *Hv*CSLF10) have been shown to synthesize a β-1,4-linked glucoxylan polymer, indicating that a single CSL family can possess multiple synthetic activities (Little et al., 2019). However, the functions of *CSLD*s and the other *CSL* families (CSLB, CSLE, CSLG) remain poorly characterized (Scheible and Pauly, 2004).

CSLD proteins were initially proposed to synthesize cellulose in tip-growing pollen tubes, consistent with the high degrees of sequence similarity and overall domain organization CSLDs share with CESAs (Doblin et al., 2001). Confirming an important role in tip-restricted cell expansion, Arabidopsis *CSLD2* and *CSLD3* are required for proper root hair growth, and *csld1* and *csld4* mutants are male sterile, presumably due to defects in pollen tube growth (Favery et al., 2001; Wang et al., 2001; Bernal et al., 2008). The functional roles of CSLD enzymes are not restricted solely to cells undergoing tip-restricted expansion, with CSLD2, CSLD3, and CSLD5 all participating in construction of newly forming cell walls during plant cytokinesis (Gu et al., 2016). Furthermore, CSLD5 also displays cell-cycle-specific accumulation in dividing cells (Yoshikawa et al., 2013; Gu et al., 2016; Yang et al., 2016). Cellulose polysaccharide epitopes have been observed in tip-growing root hairs and pollen tubes (Park et al., 2011; Chebli et al., 2012), and in newly forming cell plates (Miart et al., 2014), although the predominant cell wall polysaccharide in pollen and cell plates is likely the β-1,3-glucan callose (Meikle et al., 1991; Samuels et al., 1995; Ferguson et al., 1998; Chen and Kim, 2009; Drakakaki, 2015). In Arabidopsis, CSLD5 insertional mutants accumulated less xylan in stems and had reduced pectin (Bernal et al., 2007), and in a weak mutant allele of CSLD3, *rhd7*, the organization of xyloglucan and cellulose was altered in root hairs (Galway et al., 2011). Microsomal membranes isolated from tobacco (*Nicotiana benthamiana*) heterologously expressing Arabidopsis CSLD2, CSLD3, and CSLD5 proteins were shown to contain elevated mannan synthase activity, specifically utilizing GDP-mannose (GDP-Man) as an activated nucleotide-sugar donor (Verhertbruggen et al., 2011; Yin et al., 2011), and examination of cell wall epitopes in newly forming cell plates in shoot apical meristems in *csld5* mutants displayed altered β-1,4-mannan accumulation (Yang et al., 2016). Alternatively, a functional YFP-CSLD3 fusion protein localized to apical plasma membranes in the tips of growing Arabidopsis root hairs, and genetic chimeras, where the CSLD3 catalytic domain (residues 340–921) was replaced with the corresponding CESA6 catalytic domain,

rescued root hair defects in *csld3* mutant plants, supporting a UDP-glucose (UDP-Glc)-dependent CSL activity for CSLD3 (Park et al., 2011).

Here, we show using a combination of genetic and biochemical analysis, combined with in vivo localization of fluorescently tagged fusion proteins, that a Citrine-CESA6 chimeric fusion protein containing the catalytic domain of CSLD3, integrates into plasma-membrane-localized CSCs and is able to fully rescue both the hypocotyl elongation and cellulose accumulation defects in the *prc1-1* (*CESA6* null) mutant. In addition, we show that proteoliposomes containing purified CESA6 and CSLD3 utilize UDP-Glc but not GDP-Man and accumulate β-1,4-glucan when supplied with UDP-Glc, while CSLA9 instead only utilized GDP-Man. These results are further supported by computational modeling and simulation of substrate binding for CESA6, CSLD3, and CSLA9 enzymes. Finally, both CESA6 and CSLD3 proteins could be purified as higher-order complexes, which form ~10- to 12-nm particles with apparent threefold symmetry when examined by electron microscopy.

RESULTS

A Genetic Chimera with a CSLD3 Domain Restores CESA Functions in *cesa6* Mutants

CESA and CSLD proteins share overall membrane topology and maintain high degrees of sequence identity, especially in the central domain, where critical catalytic residues are absolutely conserved (Figure 1A; Morgan et al., 2013; Sethaphong et al., 2013; Slabaugh et al., 2014). We previously used this structural similarity to demonstrate that a fluorescently tagged chimeric fusion protein in which the CSLD3 catalytic region was replaced with the corresponding CESA6 catalytic domain was able to quantitatively rescue *kjk-2* (*csld3* null) root hair defects (Park et al., 2011). While these results indicated that a chimeric CSLD3 fusion could restore root hair growth, it remained unclear whether CSLD catalytic domains could replace CESA sequences. To address this, we generated stably transformed Arabidopsis lines expressing a fluorescently tagged Citrine-CESA6 chimera containing a CSLD3 catalytic

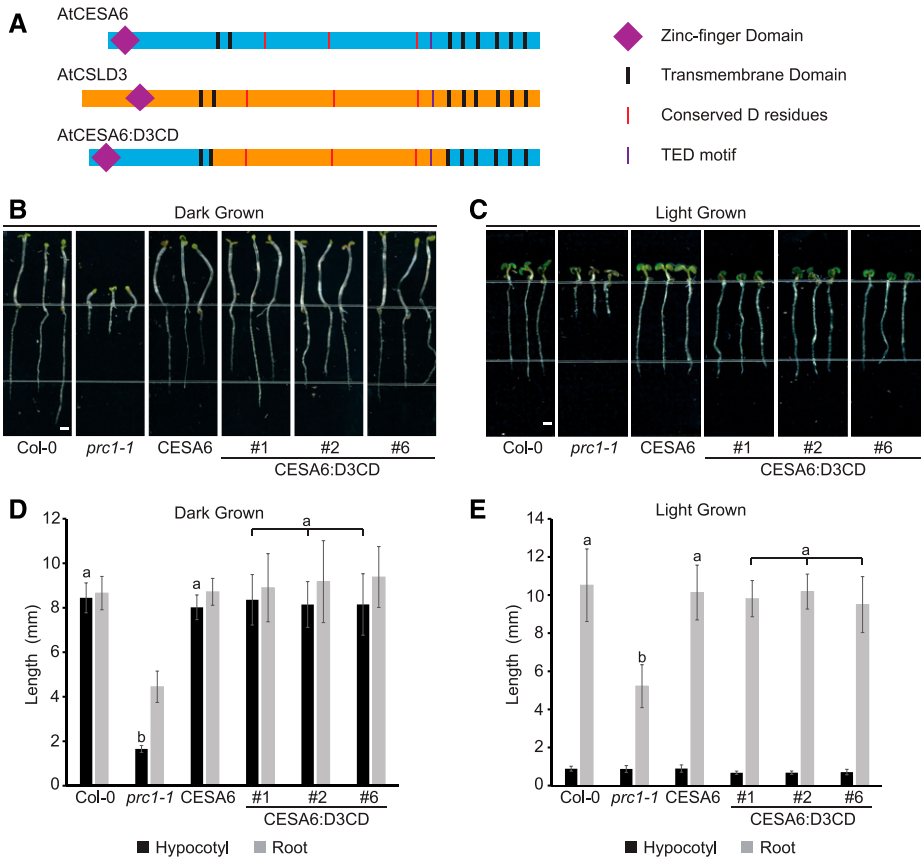

Figure 1. Expression of Citrine-CESA6:D3CD Chimera Proteins Driven by CESA6 Promoter Fully Rescues *cesa6* Hypocotyl Elongation Defects.

(A) Schematic diagram of CESA6 (blue), CSLD3 (orange), and the chimeric CESA6:D3CD protein structures. Five-day-old seedlings grown in darkness **(B and D)** and light **(C and E)** were analyzed and measured by Fiji-ImageJ (Schindelin et al., 2012). The *cesa6*$^{prc1-1}$ mutants displayed both hypocotyl and root elongation defects when compared with *Col-0* **(D and E)**. Independently transformed plants expressing either YFP-CESA6 **(**lane 3 in **B and C)** or Citrine-CESA6:D3CD proteins **(**lanes 4, 5, and 6 in **B and C)** in the *cesa6*$^{prc1-1}$ mutant background quantitatively restored hypocotyl and root elongation to wild-type levels **(D and E)**. Twelve individual plants were measured for each group. Scale bar in **(B)** and **(C)**, 1 mm. Error bars in **(D)** and **(E)** represent SD. Labels a, b indicate significantly different groups; $P < 0.05$ (one-way ANOVA).

region (Citrine-CESA6:D3CD) under control of the endogenous CESA6 promoter (Figure 1A). The CESA6 chimera quantitatively rescued both dark-grown hypocotyl elongation defects (Figures 1B and 1D) and root elongation defects observed in *cesa6* (*prc1-1*) mutant plants grown either in the dark (Figures 1B and 1D) or in light (Figures 1C and 1E), indicating CSLD3 catalytic domain sequences could functionally replace CESA6 catalytic domain sequences in the CESA6 primary cell wall CESA protein.

In plants, CESAs organize into multimeric CSCs that can be visualized as discrete fluorescent particles that display linear motility within the plasma membrane (Paredez et al., 2006; Desprez et al., 2007). To determine whether Citrine-CESA6:D3CD chimeric proteins were present in motile CSCs, we performed

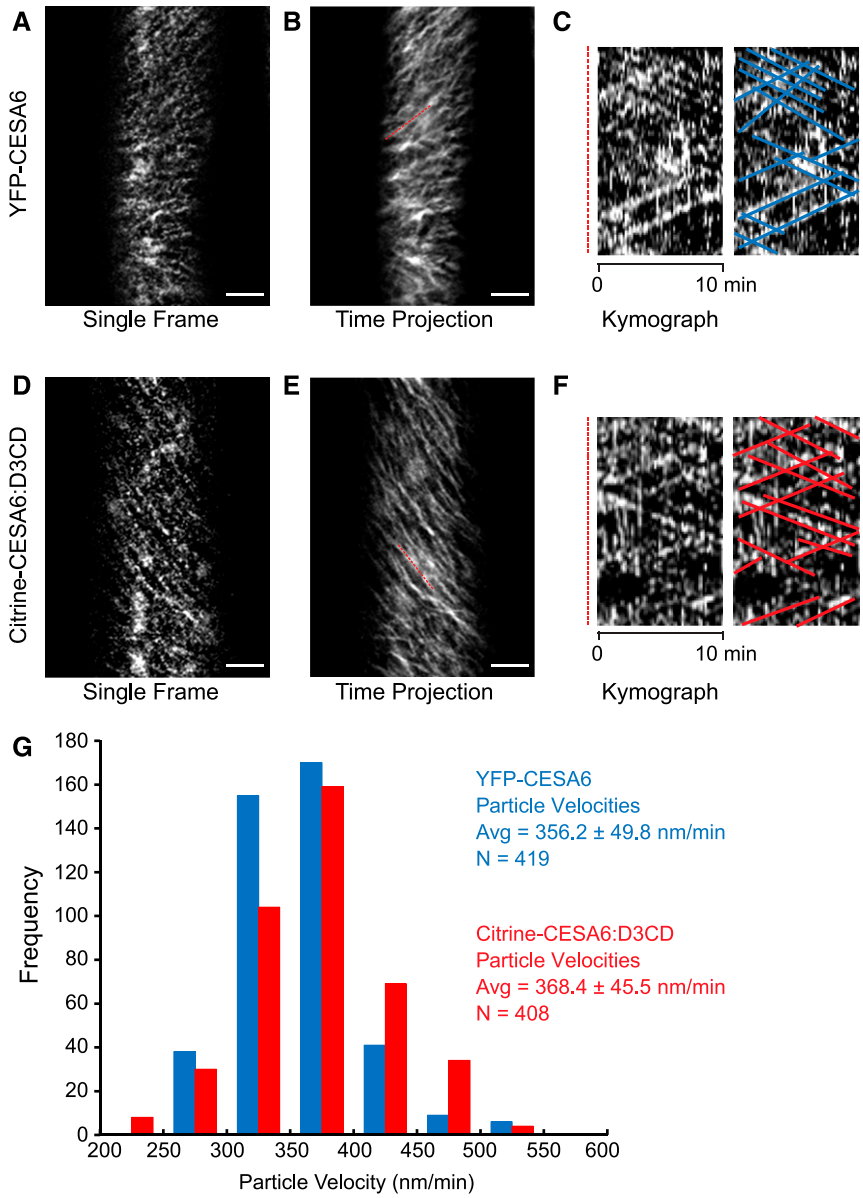

Figure 2. Citrine-CESA6:D3CD Chimeric Proteins Integrate into CSC Complexes and Display Similar Mobility as CSCs Containing YFP-CESA6.

Confocal laser-scanning microscopy was performed on hypocotyl epidermal cells of 3-d-old dark-grown seedlings. Fluorescent CSC particles containing YFP-CESA6 were observed and presented as **(A)** single frame, **(B)** time-lapse projection, and **(C)** a time-resolved kymograph of region labeled in red dashed line in **(B)**.

(D) Single frame, **(E)** time-lapse projection, and **(F)** kymograph of red dashed line in **(E)** of Citrine-CESA6:D3CD, respectively. Scale bar, 5 μm. Blue lines **(C)** and red lines **(F)** represent the tracks of YFP-CESA6- and Citrine-CESA6:D3CD-labeled particles, respectively.

(G) Histogram showed the distribution of particle velocities labeled by YFP-CESA6 (blue), calculated from 419 particles in seven individual seedlings (nine cells total) and Citrine-CESA6:D3CD (red), calculated from 408 particles in six individual seedlings (nine cells total).

time-lapse laser-confocal microscopy and investigated CSC motility in time-averaged projections in plants stably expressing either YFP-CESA6 (Figures 2A to 2C; Supplemental Movie 1) or Citrine-CESA6:D3CD (Figures 2D to 2F; Supplemental Movie 2). CSC particle trajectories were observed for both YFP-CESA6 (Figure 2C, blue lines in right) and Citrine-CESA6:D3CD chimera proteins (Figure 2F, red lines in right). Speeds calculated for YFP-CESA6 containing CSCs (Figure 2G, blue bars; 10 cells, seven seedlings, 419 particles) were virtually indistinguishable from Citrine-CESA6:D3CD containing CSCs (Figure 2D, red bars; 11 cells, six seedlings, 408 particles) at 356.2 ± 49.8 nm/min and 368.4 ± 45.5 nm/min, respectively. While these velocities are somewhat faster than the speeds of ~250 to 300 nm/min reported in several previous studies (DeBolt et al., 2007; Vain et al., 2014; Watanabe et al., 2018), others have reported higher particle velocities of ~350 to 400 nm/min (Paredez et al., 2006; Gutierrez et al., 2009; Li et al., 2012; Lei et al., 2014), which are consistent with the velocities we detected. These results indicate that Citrine-CESA6:D3CD chimera proteins are capable of integrating into primary cell wall CSCs and, based on their similar speeds, display similar cell wall biosynthesis characteristics.

Earlier genetic studies indicated that at least three distinct CESA proteins are required for cellulose synthesis during primary cell wall formation, and therefore CSCs involved in primary cell wall cellulose synthesis are thought to assemble with both essential CESAs, CESA1 and CESA3, and at least one of either CESA6 or CESA2/5/9 (Arioli et al., 1998; Fagard et al., 2000; Scheible and Pauly, 2004). To test whether motile CSCs containing Citrine-CESA6 and Citrine-CESA6:D3CD also contain other CESAs implicated in cellulose synthesis in primary cell walls, transgenic Arabidopsis expressing these fluorescent CESA6 fusions as well as GFP-CESA3 (Desprez et al., 2007) were generated and analyzed by laser-scanning confocal microscopy. Fluorescence signals specific for either Citrine/YFP or GFP (Supplemental Figure 1) were collected simultaneously from plants expressing GFP-CESA3 and either YFP-CESA6 (Figure 3A) or Citrine-CESA6:D3CD (Figure 3C). Significant overlap of GFP-CESA3 (Figures 3A and 3C, green) and either YFP-CESA6 (Figure 3A, magenta) or Citrine-CESA6:D3CD (Figure 3C, magenta) signals were observed. When relative fluorescence intensity values for individual CSC particles were examined, significant coincident fluorescence could be observed for GFP-CESA3 (Figures 3B and 3D, green) and either YFP-CESA6 (Figure 3B, magenta) or Citrine-CESA6:D3CD (Figure 3D, magenta), indicating that both fluorescently tagged CESA6 and CESA6:D3CD proteins occur in multimeric CSCs with other CESA proteins.

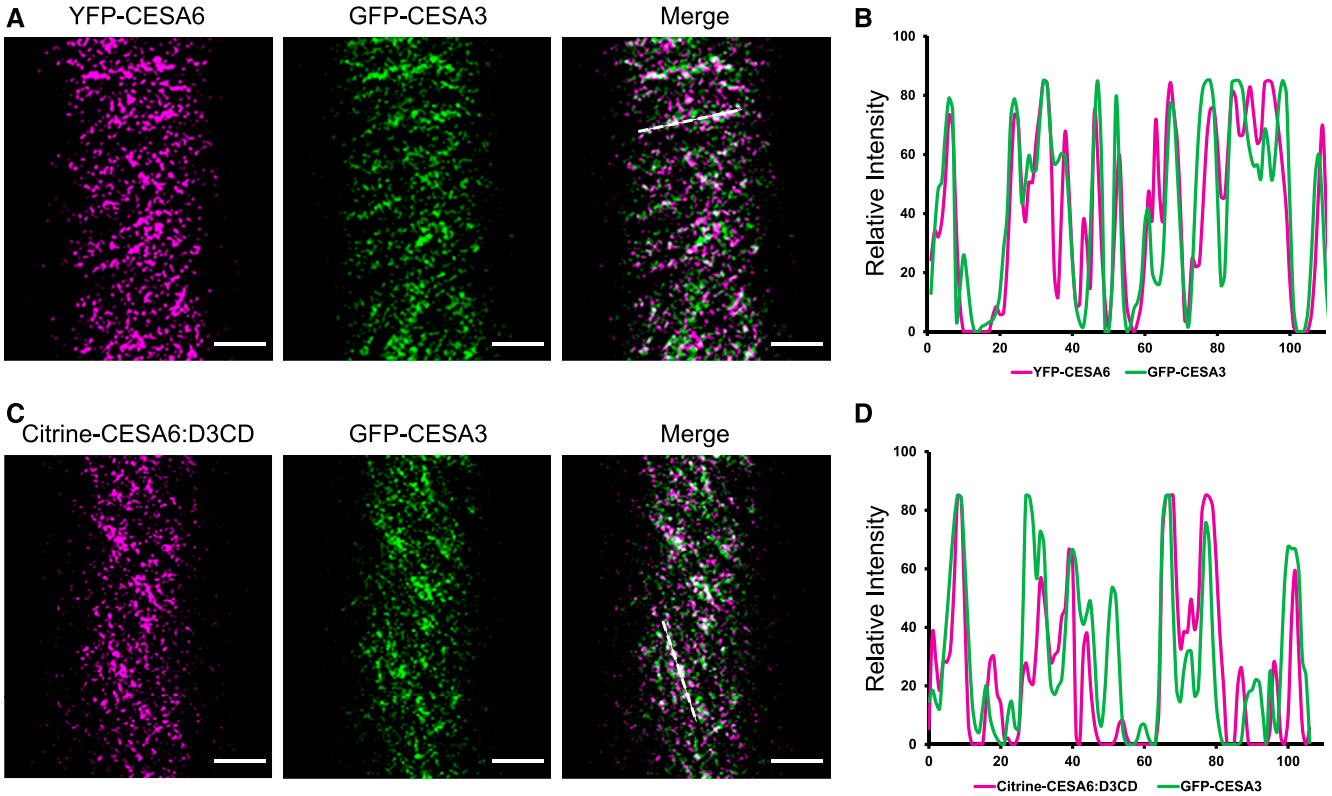

Figure 3. Citrine-CESA6:D3CD Chimeric Proteins Colocalize with GFP-CESA3 Proteins and Integrate into the Same CSC Complexes.

Three-day-old dark-grown F2 seedlings expressing both YFP-CESA6 and GFP-CESA3 were imaged by simultaneous two-channel confocal microscopy.
(A) Single frame of YFP-CESA6 (magenta), GFP-CESA3 (green), and a merged image.
(B) Plot of relative intensity through the white dashed line in **(A)** showing a strong association between the localization of YFP-CESA6 and GFP-CESA3.
(C and D) Single frame and plot of relative intensity of F2 seedlings expressing both Citrine-CESA6:D3CD (magenta) and GFP-CESA3 (green), respectively.
Scale bar in **(A)** and **(C)**, 5 μm.

While these results supported the integration of Citrine-CESA6:D3CD chimeras into CSCs and rescue of *prc1-1* mutant phenotypes, they did not directly address whether the Citrine-CESA6:D3CD chimera was catalytically active or simply allowed for assembly of complexes with nonfunctional subunits. To address this directly, we mutated a conserved TED motif responsible for formation of β-1,4-glucosidic bonds in the extending glucan polymers (Morgan et al., 2013, 2016), replacing both Asp and Glu with Ala residues. Neither stably transformed Citrine-CESA6-TAA nor Citrine-CESA6:D3CD-TAA plants were able to fully rescue dark-grown hypocotyl and root elongation defects (Figures 4A and 4B; Supplemental Figure 2). Interestingly, while Citrine-CESA6:D3CD-TAA-expressing plants were indistinguishable from *prc1-1* mutants, we did observe a small, statistically significant increase in dark-grown hypocotyl length in seedlings expressing the Citrine-CESA6-TAA protein (~15%; Figures 4A and 4B). Quantification of crystalline cellulose in these seedlings using the Updegraff method confirmed that expression of both YFP-CESA6 and Citrine-CESA6:D3CD restored crystalline cellulose content to wild-type levels (Figure 4C), while cellulose content of Citrine-CESA6:D3CD-TAA seedlings was indistinguishable from that of the *prc1-1* mutant background. Interestingly, consistent with earlier phenotypic analysis (Figures 4A and 4B), we also observed a small, statistically relevant increase in crystalline cellulose content in the Citrine-CESA6-TAA-expressing seedlings (Figure 4C). Taken together, these results strongly support the interpretation that the quantitative rescue of *prc1-1* mutant phenotypes and chemotypes observed in seedlings expressing YFP-CESA6 and Citrine-CESA6:D3CD chimeras requires the catalytic function of a β-1,4-glucan synthase.

While the introduction of point mutations in both Citrine-CESA6-TAA and Citrine-CESA6:D3CD-TAA mutants are unlikely to affect overall folding of these proteins, we wanted to address whether these mutant proteins also associated into CSCs in these transgenic seedlings and whether these "catalytically dead" constructs displayed any differences in either CSC trafficking or dynamics in these plants. As with their wild-

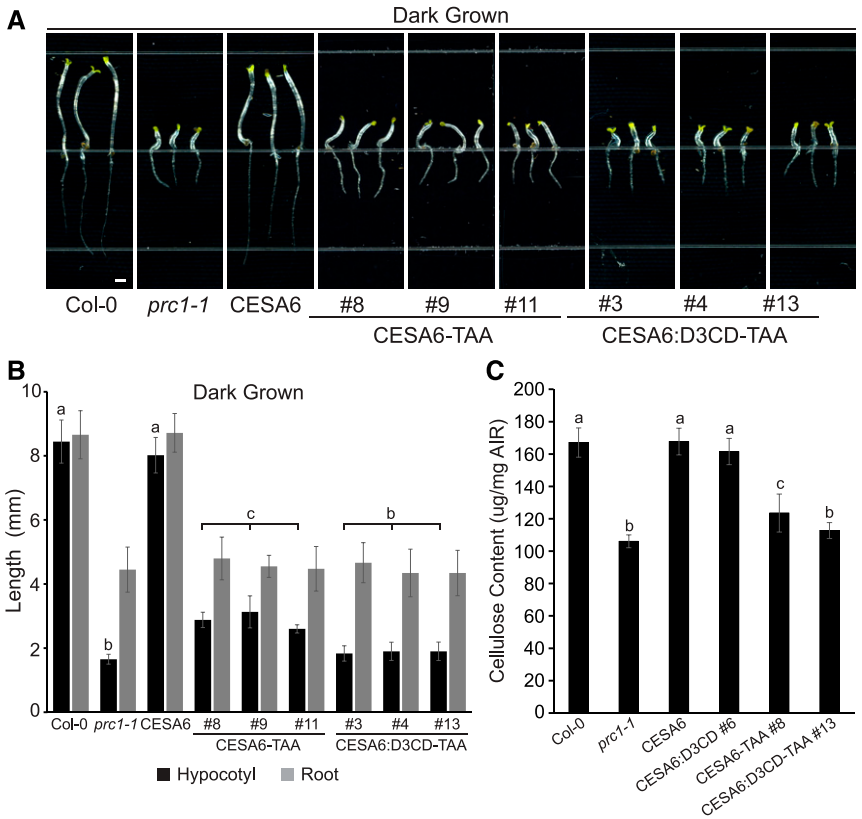

Figure 4. Citrine-CESA6 and Citrine-CESA6:D3CD Proteins Must Be Catalytically Active to Rescue *cesa6* Hypocotyl Elongation Defects.

(A) Five-day-old dark-grown seedlings were analyzed and measured by ImageJ. Three independent transgenic lines expressing either Citrine-CESA6-TAA (nos. 8, 9, and 11) or Citrine-CESA6:D3CD-TAA (nos. 3, 4, and 13) failed to rescue *cesa6*$^{prc1-1}$ hypocotyl elongation defects. Quantification shown in **(B)**. **(C)** Crystalline cellulose content of 10-d-old seedlings was measured using Updegraff methods on alcohol insoluble residue (AIR). The cellulose content of the *cesa6*$^{prc1-1}$ mutant was reduced compared with Col-0. This deficiency was rescued in both YFP-CESA6 and Citrine-CESA6:D3CD (CESA6:D3CD line no. 6, from Figure 1) seedlings, but not in Citrine-CESA6-TAA (CESA6-TAA line no. 8, in **A**) and Citrine-CESA6:D3CD-TAA (CESA6:D3CD-TAA line no. 13, in **A**) transgenic lines. Scale bar in **(A)**, 1 mm. Error bars in **(B)** and **(C)** represent SD. Labels a, b, and c indicate significantly different groups; $P < 0.05$ (one-way ANOVA).

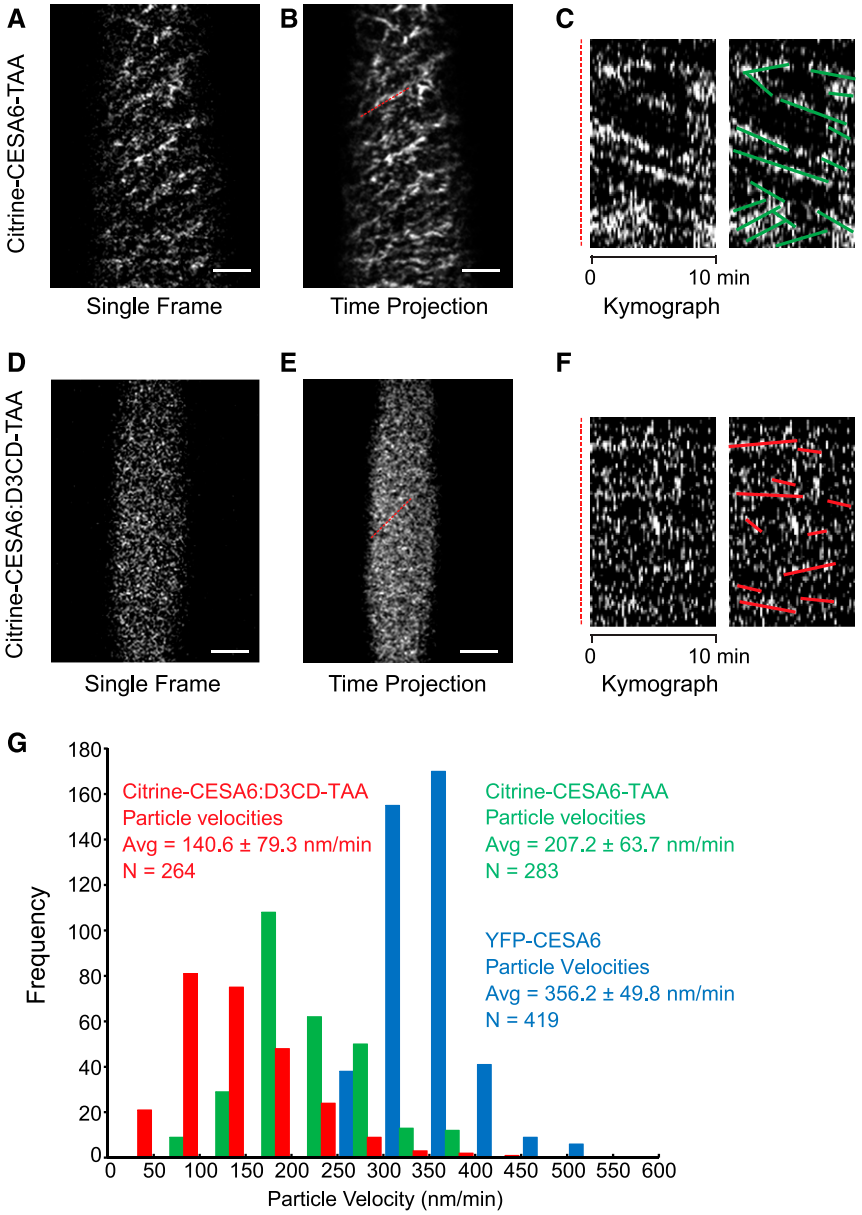

Figure 5. TAA Mutants of Citrine-CESA6 and Citrine-CESA6:D3CD Integrate into CSCs but Display Altered Mobility Compared with Functional Complexes.

(A) Single frame, **(B)** time-lapse projection, and **(C)** kymograph of red dashed line in **(B)** of Citrine-CESA6-TAA-containing CSCs imaged by confocal scanning microscopy of 3-d-old dark-grown seedlings.

(D) Single frame, **(E)** time-lapse projection, and **(F)** kymograph of red dashed line in **(E)** of Citrine-CESA6:D3CD-TAA-containing CSCs. Scale bar, 5 μm. Green lines **(C)** and red lines **(F)** represent the tracks of Citrine-CESA6-TAA- and Citrine-CESA6:D3CD-TAA-labeled particles, respectively.

(G) Histogram showing the relative distribution of particle velocities labeled by both Citrine-CESA6-TAA (green), calculated from 283 particles in 6 individual seedlings (6 cells total), and Citrine-CESA6:D3CD-TAA (red), calculated from 264 particles in 8 individual seedlings (8 cells total). YFP-CESA6 (blue) particle velocities (reproduced from Fig 2G) are presented as reference.

type counterparts, both Citrine-CESA6-TAA (Figures 5A to 5C; Supplemental Movie 3) and Citrine-CESA6:D3CD-TAA (Figures 5D to 5F; Supplemental Movie 4) proteins were incorporated into discrete CSC particles in the plasma membrane of Arabidopsis hypocotyl cells at generally similar densities as observed for catalytically active versions of these proteins (Figure 5; Supplemental Figure 3). To assess whether either the presence of a CSLD3 catalytic domain in chimeric proteins or TAA point mutations affected the assembly and delivery of CESA6-containing CSCs to plasma membranes, we examined rates at which fluorescently labeled CSCs appeared in a photobleached plasma membrane region for CSC complexes containing YFP-

CESA6, Citrine-CESA6:D3CD, Citrine-CESA6-TAA, and Citrine-CESA6:D3CD-TAA (Supplemental Figures 3A to 3D, red boxes). For all constructs, we observed similar rates of delivery of new, fluorescently labeled CSCs, indicating that the assembly of CESA6-containing CSCs and their delivery to plasma membranes were not significantly affected (Supplemental Figures 3E and 3F). However, when we examined CSC motility events, we observed that particle tracks containing Citrine-CESA6-TAA were markedly shorter than those containing YFP-CESA6 (Figures 5A to 5C; green lines in Figure 5C, right), and CSC particles containing Citrine-CESA6:D3CD-TAA were virtually immobile (Figures 5D to 5F; red lines in Figure 5F, right). Speeds calculated for CSC motility events for particles containing TAA point mutations in their catalytic domains were also significantly slower than their catalytically active counterparts, with Citrine-CESA6-TAA particle speed reduced to 207.2 ± 63.7 nm/min (Figure 5G, green bars; six cells, six seedlings, 283 particles) and Citrine-CESA6:D3CD-TAA to 142.3 ± 87.5 nm/min (Figure 5G, red bars; six cells, six seedlings, 253 particles). All together, these results confirm that "catalytically dead" Citrine-CESA6-TAA and Citrine-CESA6:D3CD-TAA subunits successfully integrate into CSCs and are delivered to plasma membranes in rates largely indistinguishable from their catalytically active counterparts. However, CSCs containing these TAA mutant subunits show distinctly slower particle speeds and dramatically shorter particle trajectories, consistent with the impaired rescue of *prc1-1* phenotypes and cellulose deposition observed earlier (Figure 4).

Purification and Reconstitution of Catalytically Active CSLD3, CESA6, and CSLA9 Enzymes into Proteoliposomes

While the in vivo rescue of cell wall defects in the CESA6 mutant *prc1-1* is consistent with a UDP-Glc-dependent β-1,4-glucan synthase activity for CSLD proteins, earlier studies of isolated *N. benthamiana* microsomal membranes overexpressing CSLD proteins identified increased GDP-Mandependent β-1,4-mannan synthase activities (Verhertbruggen et al., 2011; Yin et al., 2011). To directly test whether CSLD proteins utilize UDP-Glc to synthesize β-1,4-glucan or GDP-Man to synthesize β-1,4-mannan, we generated His-tagged versions of CSLD3, as well as CESA6 and CSLA9, which were used as a positive and negative controls for UDP-Glc- and GDP-Man-dependent polysaccharide synthase activities. These cell wall synthases were expressed in *Saccharomyces cerevisiae* under control of a galactose-inducible promoter (Figure 6A).

While *S. cerevisiae* do not contain β-1,4-glucans, they do contain significant amounts of β-1,3-glucan and chitin (β-1,4-linked GlcNAc) polysaccharides in their cell walls and β-1,4-glucosidic linkages often connect these β-1,3-glucan and chitin polymers (Lesage and Bussey, 2006). These, or similar, endogenous yeast transglycosylase activities might therefore complicate assessment of potential β-1,4-glucan synthase activities of the heterologously expressed CESA6 and CSLD3 proteins. To more specifically assess the enzymatic activities of these plant cell wall synthases, microsomal membranes were isolated from yeast expressing CESA6, CSLD3, and CSLA9 and treated with a panel of

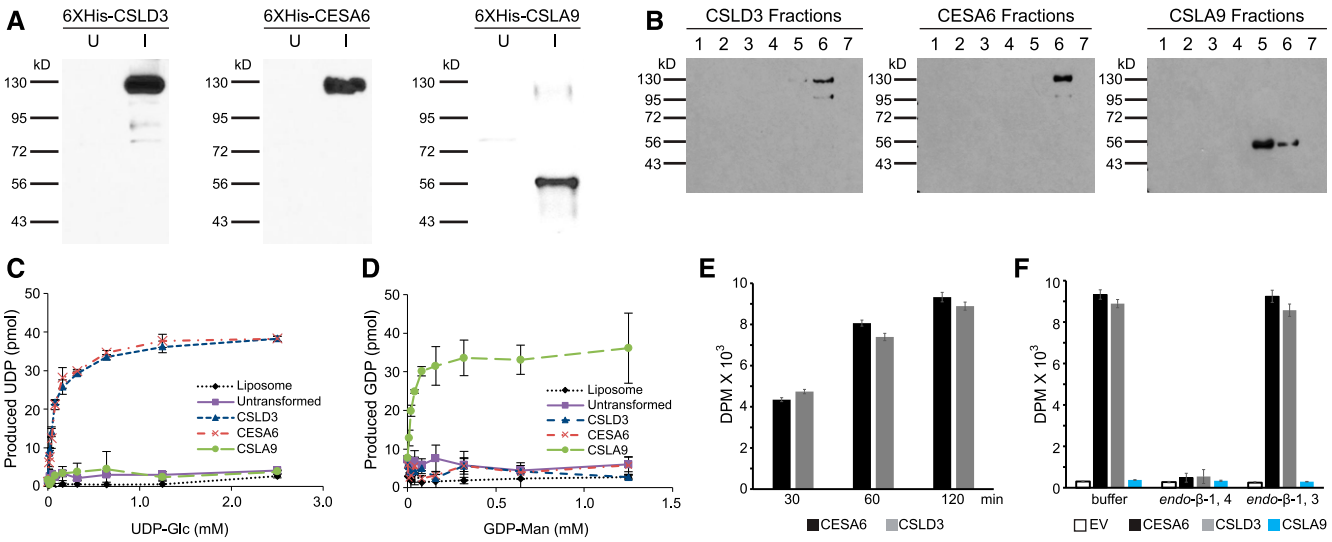

Figure 6. Detection of β-1,4-glucan Polysaccharides in Proteoliposomes Reconstituted with Purified His-CSLD3 and His-CESA6.

(A) Immunoblot analysis of yeast microsomal proteins isolated from uninduced (U) and induced (I) yeast expressing His-CESA6, His-CSLD3, and His-CSLA9. Detection with anti-His antibodies.

(B) Immunoblot analysis of proteoliposome fractions (probed with anti-His antibodies) demonstrated successful incorporation of His-CESA6, His-CSLD3, and His-CSLA9 into reconstituted proteoliposomes formed with isolated yeast lipids (fraction number shown in Supplemental Figure 4D).

(C) Proteoliposomes containing His-CSLD3 and His-CESA6 displayed saturable UDP-forming activities when supplied with UDP-Glc, while only proteoliposomes containing His-CSLA9 **(D)** displayed saturable GDP-forming activity when supplied with GDP-Man.

(E) Time-dependent β-1,4-glucan synthesis by both CESA6 and CSLD3 using UDP-[^{3}H]-glucose as tracer.

(F) Enzymatic digestion of CESA6 and CSLD3 synthesized glucan by β-1,4-endoglucanase. DPM, Disintegrations per minute; EV, empty vector. All experiments were performed in triplicate. Error bars in **(E)** and **(F)** represent SD.

nondenaturing detergents and lipid analogs to determine their ability to efficiently solubilize these proteins (Supplemental Figures 4A to 4C). Interestingly, CSLD3 and CSLA9 proteins were unable to be efficiently solubilized in the presence of the nondenaturing detergent Triton X-100 (Supplemental Figures 4A to 4C), while ~50% of CESA6 was recovered in the soluble fraction under these detergent conditions. Similarly, while CSLA9 and ~50% of CESA6 were solubilized in the presence of lysophosphatidylcholine, CSLD3 remained in the insoluble fraction in these conditions. These three integral membrane polysaccharide synthases were most efficiently solubilized in the presence of a pair of lipid analogs, lysoFos-Choline Ether-14 (LFCE-14), or lauryl dimethyl amine-N-oxide. As >90% of both CSLD3 and CSLA9 and around 50% of CESA6 were solubilized in the presence of LFCE-14, this detergent was used for further purification steps. Detergent-solubilized His-CSLD3, His-CESA6, and His-CSLA9 protein fractions were enriched by affinity purification on Ni-agarose columns (Supplemental Figures 5A to 5C). Purified His-CSLD3, His-CESA6, and His-CSLA9 were mixed with *S. cerevisiae* total lipid extracts, and reconstituted proteoliposomal fractions containing purified cell wall polysaccharide synthases were isolated using sucrose density gradient ultracentrifugation (Supplemental Figure 5D). The presence of His-tagged CSLD3, CESA6, and CSLA9 proteins in these proteoliposomes was determined by immunoblotting with anti-His antibodies (Figure 6B). Reactions catalyzed by glycosyltransferases (GTs), such as members of the CESA/CSL superfamily, are bi-substrate reactions, and the nucleotide product (UDP, GDP) can be measured to quantify GT activity. Substrate specificity and catalytic activity of these proteins were assessed in the presence of 1 mM Mn^{2+} and 1 mM Mg^{2+} and either UDP-Glc (Figure 6C) or GDP-Man (Figure 6D). When reconstituted into proteoliposomes and provided UDP-Glc, saturable UDP-forming activities were observed for both CSLD3 and CESA6 proteins, but not for CSLA9, which utilizes GDP-Man (Figures 6C and 6D). The apparent K_m values of CSLD3 and CESA6 for UDP-Glc were 65 μM and 73 μM, respectively, consistent with values recently reported for reconstituted PttCESA8 (~30 μM; Purushotham et al., 2016) and significantly lower than values determined for the bacterial CESA, RsBCSA (~500 μM; Omadjela et al., 2013). When reconstituted proteoliposomes were provided with GDP-Man, saturable GDP-forming activities (K_m value of 17 μM) were only observed in proteoliposomal fractions containing the β-1,4-mannan synthase, CSLA9, but not for either CSLD3 or CESA6 (Figure 6D). Both UDP-forming activities for CESA6 and CSLD3 proteins and GDP-forming activities for CSLA9 were time and concentration dependent (Supplemental Figure 6).

To determine the nature of the polysaccharides produced in these reactions, proteoliposomes containing purified CESA6, CSLD3, CSLA9, and Ni^{2+}-agarose eluted proteins from an empty vector control were incubated with UDP-Glc, Mg^{2+}, and Mn^{2+} and a UDP-[^{3}H]-Glc as a tracer. Time-dependent accumulation of [^{3}H]-Glc containing reaction products were observed for both CESA6 and CSLD3 upon sedimentation and subsequent purification of insoluble reaction products by paper chromatography (Figure 6E), but not for CSLA9 or the empty vector control proteoliposomes (Figure 6F). To determine whether in vitro-synthesized material represented β-1,4 glucan, these reaction products were incubated with glucanases specifically degrading β-1,3-linked or β-1,4-linked glucans. Consistent with the formation of cellulose, both CESA6 and CSLD3 reaction products were selectively degraded only by a β-1,4-specific glucanase and were largely resistant to treatment with a β-1,3-specific glucanase (Figure 6F). Although fibrillar structures, structurally similar to cellulose microfibrils, were observed in recent reconstitution experiments with plant CESAs (Purushotham et al., 2016; Cho et al., 2017), we were unable to detect similar fibrils in reconstituted proteoliposome fractions with either CESA6 or CSLD3. Taken together, these results strongly support the conclusion that CSLD3 utilizes UDP-Glc as a substrate and synthesizes β-1,4-glucan and not β-1,4-mannan.

To further understand how UDP-Glc and GDP-Man substrates might be selectively bound within CSLD, CESA, and CSLA catalytic domains, we generated 3D atomistic models of the cytosolic catalytic domains of CSLD3, CESA6, and CSLA9 (Liepman et al., 2005; Goubet et al., 2009). These structural models were based on the recently solved crystal structures of bacterial CESA, RsBCSA (Morgan et al., 2013, 2016). RsBCSA, like plant CESA and CSL family proteins, is a member of the conserved GT2 superfamily. While sequence identity between RsBCSA and CSLD3, CESA6, and CSLA9 proteins are relatively dissimilar overall, conservation of the catalytic domains is higher (31.5%, 30.0%, and 27.6% identity for CSLD3, CESA6, and CSLA9, respectively), and previous structural alignments have shown that the core catalytic domain of plant CESA and CSLD proteins show significant structural similarities (Sethaphong et al., 2013; Li et al., 2017). Arabidopsis CSLD3 (Uniprot Q9M9M4), CESA6 (Uniprot Q94JQ6), and CSLA9 (Uniprot Q9LZR3; UniProt Consortium, 2019) were aligned with the catalytic region of RsBCSA (PDB ID: 5EIY, chain A) using the SWISS-MODEL webserver (Guex et al., 2009; Benkert et al., 2011; Bertoni et al., 2017; Bienert et al., 2017; Waterhouse et al., 2018). CSLD3, CESA6, and CSLA9 models all showed substantial structural conservation when aligned with the RsBCSA crystal structure, with the exception of two plant-specific plant-conserved (PCR) and class-specific regions (CSR) that displayed randomly disordered structures (Supplemental Figure 7A). However, these domains, which are suspected to participate in rosette complex formation (Sethaphong et al., 2013), are too far away from the enzyme activity sites to substantially influence substrate binding in the highly conserved structural cores of these catalytic domains.

To identify additional amino acid residues that might participate in binding of nucleotide sugar substrates, we initially focused on amino acids whose 3D positions were within seven angstroms of the bound UDP-Glc in the crystal structure of BCSA, and compared this with the 3D structural models (Supplemental Figure 7A, blue spheres). These amino acid sequences from RsBCSA, CESA6, CSLD3, and CSLA9 were aligned with the other Arabidopsis CESA, CSLD, and CSLA family members (Supplemental Figure 7B). In addition to the conserved GT2 catalytic motifs, additional amino acids within the CESA and CSLD binding pockets were highly conserved with one another and not with CSLA proteins, possibly reflecting differing nucleotide-sugar binding specificities. When UDP-Glc binding was modeled with RsBCSA, the UDP-Glc consistently adopted a binding mode in a conformation similar to that

observed in the RsBCSA crystal structure (average root-mean-square-deviation 0.8 Å; Supplemental Figure 7C; Supplemental Movie 5). Interestingly, while UDP-Glc consistently adopted binding characteristics similar to those observed for BCSA in CESA6 and CSLD3 binding simulations (Supplemental Figure 7C; Supplemental Movie 5), in CSLA9, UDP-Glc consistently assumed a different "closed" conformation (Supplemental Figure 7C; Supplemental Movie 6). Instead, in CSLA9 simulations, GDP-Man bound in an "open" conformation (Supplemental Figure 7D; see Supplemental Movie 6), while assuming "closed" conformations in RsBCSA, CESA6, and CSLD3 GDP-Man (Supplemental Figure 7D; Supplemental Movie 7). Intriguingly, stabilization of the "open" conformation of the GDP-Man in the CSLA9 binding simulation involved interaction with an aromatic trio of Trp-451, Phe-106, and Tyr-171 (Supplemental Figure 7B, bold red amino acids). These three aromatic residues are highly conserved in land plant CSLA sequences (Supplemental Figure 7E, bold red amino acids). Taken together, these results indicate that nucleotide-sugar binding pockets are more highly conserved between CESA and CSLD proteins than CSLA proteins. Additionally, the presence of several conserved aromatic residues in CSLA binding pockets may be associated with GDP-Man nucleotide-sugar selection in these enzymes.

Detergent Solubilized CSLD3 and CESA6 Proteins Assemble into Higher-Order Complexes

In plants, β-1,4-glucans synthesized by plant CESA proteins coalesce into microfibrils of 18 to 24 individual glucan polymers held together via hydrogen bonding (Cosgrove, 2018). This efficient microfibril bundling is thought to occur due to the assembly of higher-order CSCs, comprised of at least three CESAs organized into subcomplexes that then further associate into six-lobed rosettes (Polko and Kieber, 2019). The ability to detect UDP-Glc-dependent formation of β-1,4-glucan polysaccharides in reconstituted proteoliposomes containing CSLD3 and CESA6 (Figure 6) suggested that these detergent-solubilized protein complexes maintain appropriate conformation during their isolation and purification. We were interested therefore in whether the detergent-solubilized His-CESA6, His-CSLD3, and His-CSLA9 proteins might also be found in higher-order complexes. Detergent-solubilized complexes were therefore separated by size-exclusion chromatography, and resulting fractions were analyzed by SDS-PAGE and immunoblotting with anti-His antibodies (Figure 7A). Both His-CSLD3 and His-CESA6 eluted as high-molecular-weight complexes with estimated sizes significantly larger than the ~700-kD thyroglobulin complexes observed in molecular weight standards typically used for analysis of globular protein complexes (Figure 7B). While His-CSLA9 complexes also migrated as higher-order complexes, these were markedly smaller, with estimated molecular size of ~150 to 200 kD when compared with globular protein molecular weight standards.

Based on their large apparent molecular sizes, we attempted to visualize these purified, detergent-solubilized CSLD3 and CESA6 fractions by electron microscopy. When detergent-solubilized membrane fractions from untransformed yeast, and yeast expressing either His-CSLD3 or His-CESA6 were affinity purified, placed on electron microscopy (EM) grids, negatively stained, and imaged at 50,000× magnification, clear enrichment of ~10- to 12-nm particles in the CSLD3 and CESA6 fractions was observed (Figure 7C). When examined at higher magnification, these particles often displayed structural detail reminiscent of a "wagon-wheel," with a bright central mass often surrounded by three pairs of smaller circular structures oriented at roughly 120-degree intervals around the central mass (Figures 7B and 7C, insets).

DISCUSSION

Plant cells are surrounded by a load-bearing cell wall comprised of cellulose, hemicelluloses, pectins, and a variety of cell wall proteins (Cosgrove, 2005). CESA proteins are contained within a larger superfamily of CSL proteins (Richmond and Somerville, 2000). While a number of different biosynthetic activities have been proposed for members of the CSLD family of glycan synthases (Doblin et al., 2001; Bernal et al., 2008; Park et al., 2011; Verhertbruggen et al., 2011; Yin et al., 2011), here we present multiple lines of evidence that support classification of members of the CSLD family as β-1,4-glucan synthases. Using a genetic rescue approach, we demonstrated that a CESA6 protein chimera in which the CESA6 catalytic domain is replaced with CSLD3 catalytic sequences (CESA6:D3CD) fully rescues *cesa6* mutant alleles (Figures 2 and 4C). We had previously reported that a CSLD3 protein chimera containing a CESA6 catalytic domain could rescue *csld3* null mutant phenotypes consistent with CSLD3 being a β-1,4-glucan synthase (Park et al., 2011). However, it remained unclear whether CSLD proteins assembled into higher-order protein complexes or if β-1,4-glucan polymers generated by CSLD enzymes could produce microfibrillar cellulose. YFP-CESA6 has been observed to organize into punctate structures similar to CSCs (Paredez et al., 2006; Gutierrez et al., 2009), and loss of CESA6 activity in the *prc1* null mutant results in plants that produce less crystalline cellulose (Fagard et al., 2000; MacKinnon et al., 2006). Quantitative genetic rescue of *prc1* mutant phenotypes by Citrine-CESA6:D3CD chimeras (Figure 1) and restoration of crystalline cellulose content back to wild-type levels (Figure 4C) strongly supports the conclusion that the CSLD3 catalytic domain synthesizes β-1,4-glucan. These CESA6:D3CD chimeras integrate into CSCs (Figure 2) that also contain GFP-CESA3 (Figure 3), migrate along cortical microtubule tracks with similar speeds to YFP-CESA6-containing CSCs (Figure 2), and must be catalytically active in order to fully rescue *cesa6* mutant phenotypes (Figures 4 and 5).

The fact that Citrine-CESA6:D3CD chimeras colocalized and appear to be integrated into CSCs and were delivered to plasma membranes at similar rates as YFP-CESA6 (Supplemental Figure 3) indicates that the N-terminal and transmembrane domains of CESA6 are likely more important for assembly of these proteins into primary cell wall CSCs and for their subsequent subcellular targeting. While it is somewhat surprising that wholesale replacement of the ~70-kD CESA6 cytosolic catalytic domain with CSLD3 sequences does not affect this assembly, this may perhaps be mitigated because the CESA6 position in primary cell wall CSCs may alternatively be occupied by CESA2 and CESA5 (Desprez et al., 2007). The presence of PCRs and CSRs has been proposed to play important roles in the assembly of plant CESAs into primary and secondary cell-wall-specific CSCs (Vergara and

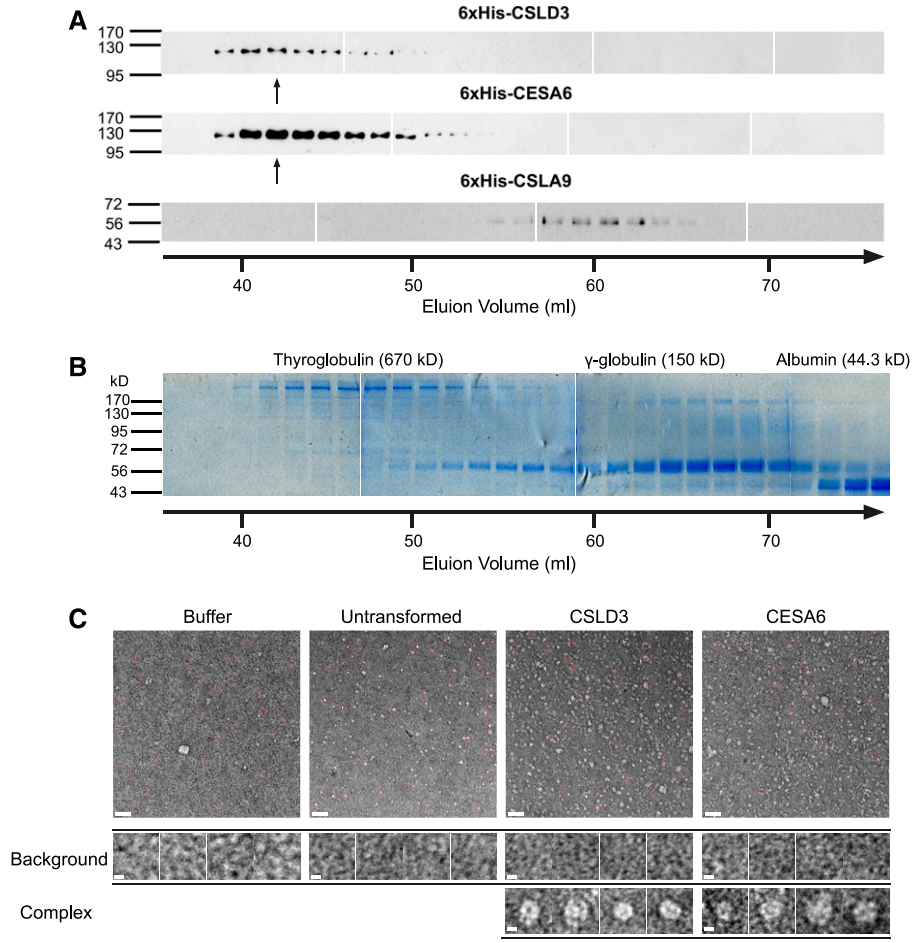

Figure 7. Detergent-Solubilized His-CSLD3 and His-CESA6 Proteins Are Found in Higher-Order Complexes.

(A) Detergent solubilized, affinity-purified His-CSLD3, His-CESA6, and His-CSLA9 proteins were separated by size-exclusion chromatography on a Sephacryl S300 16/60 column, and eluted fractions were analyzed by SDS-PAGE followed by immunoblotting with anti-His antibodies.
(B) Globular protein molecular weight standards (thyroglobulin, ~670 kD; γ-globulin, ~150 kD; and albumin, ~44.3 kD) were separated by size-exclusion chromatography on a Sephacryl S300 16/60 column. Fractions were analyzed by SDS-PAGE followed by Coomassie blue staining.
(C) Proteins present in high-molecular weight fractions (arrows in **A**) were placed on EM grids, negatively stained, and imaged by transmission electron microscopy (magnification, 50,000×). Particles with a cross-sectional diameter of ~10 to 12 nm (see enlarged insets) were enriched in both His-CSLD3- and His-CESA6-containing fractions. Scale bars, 20 nm (large panels) and 5 nm (small panels).

Carpita, 2001; Scavuzzo-Duggan et al., 2018). At least in the case of integration of the Citrine-CESA6:D3CD into primary CSCs, the absence of CESA6-specfic PCR and CSR domains does not appear to interfere with their assembly into CSCs, although the presence of similar PCR and CSR sequences in CSLDs may perhaps indicate the general ability of CSLD proteins to also assemble into higher-order protein complexes. Similarly, the absence of the cytosolic CESA6 catalytic domain does not appear to negatively affect movement of these CSCs along characteristic linear tracks (Figure 2), indicating that replacement with the CSLD3 sequences does not significantly alter interaction of these CSCs with cellulose-microtubule uncoupling (Liu et al., 2016) and cellulose-synthase-interacting proteins (CSI1/POM-POM2 and CSI3; Bringmann et al., 2012; Li et al., 2012; Lei et al., 2013), which mediate interactions between cortical microtubules and CSCs.

While rescue of hypocotyl growth defects and accumulation of crystalline cellulose required a catalytically active cytosolic domain in either YFP-CESA6 or Citrine-CESA6:D3CD proteins (Figure 4), replacement of glutamate and aspartate residues in the catalytic Thr-Asp-Glu (TED) motif with alanines (TAAs) did not appear to affect assembly of CSCs or their delivery to the plasma membrane. However, motility of Citrine-CESA6-TAA and Citrine-CESA6:D3CD-TAA containing CSCs along microtubule tracks were significantly affected, with the speed of Citrine-CESA6-TAA containing CSCs reduced by roughly one-third and Citrine-CESA6:D3CD-TAA CSCs by slightly more (Figure 5). These reduced speeds are consistent with the proposal that microtubule-associated motility is primarily driven by biosynthetic activity and the elongation and assembly of β-1,4-glucan polymers into cellulose microfibrils (Paredez et al., 2006), with a loss of catalytic activity in the CESA6 positions resulting in an associated reduction

of ~1/3 of the particle velocity. Interestingly, in addition to reduced particle velocities, we also noted a reduction in the overall length of linear tracks in CSCs containing TAA mutant subunits, perhaps indicating that "pausing" caused by catalytically inactive CESA6 may increase the chance of disengagement with cortical microtubules and/or endocytosis from the plasma membrane.

Based on genetic reconstitution experiments, as well as biochemical reconstitution of CSLD3 activity in vitro, the catalytic domain of CSLD3 appears to prefer UDP-Glc. These studies further support the synthesis of β-1,4-glucan polymers that can integrate into crystalline cellulose. Both of these activities are consistent with a β-1,4-glucan synthase activity for CSLD3, which we directly confirmed using a combination of heterologous expression in *S. cerevisiae* (Supplemental Figures 4 and 5) and in vitro reconstitution experiments with purified CESA6, CSLD3, and CSLA9 proteins (Figure 6). These results are also consistent with the recent determination that overexpression of a *Gossypium hirsutum* CSLD3 (GhCSLD3) is able to rescue cell expansion and cell wall integrity defects in Arabidopsis *prc1-1* mutants (Hu et al., 2019).

Interestingly, computational modeling showed that the catalytic domains of CSLD proteins displayed high degrees of structural similarity to plant and bacterial CESAs, and in molecular dynamics simulations performed with different nucleotide-sugar substrates, CESA6 and CSLD3 protein models bound UDP-Glc with conformations similar to those observed in the RsBCSA crystal structures (Morgan et al., 2013, 2016; Supplemental Figure 7; Supplemental Movie 5). High degrees of sequence similarity were observed between CSLD and CESA protein binding pockets, consistent with the binding of UDP-Glc in both these families. Significantly less conservation was observed in the binding pocket of CSLA family members, perhaps reflecting either different substrate binding specificity or different evolutionary origins proposed for the CSLA and CESA/CSLD clades of land plants (Little et al., 2018). Interestingly, potential stabilizing interactions observed in our simulations between the guanine of GDP-Man and conserved aromatic side chains (Supplemental Figure 7; Supplemental Movie 6) are similar to strong ring-stacking interactions observed between the guanine base of GDP-Man and a Tyr residue in the substrate binding pocket in the crystal structure of the *Escherichia coli* GDP-Man hydrolase (Boto et al., 2011).

A UDP-Glc substrate specificity for CSLD3 would appear to be inconsistent with recent descriptions of GDP-Man-dependent synthesis of β-1,4-mannan by CSLD proteins (Verhertbruggen et al., 2011; Yin et al., 2011). However, it should be noted that mannan synthesis in these studies was assessed in plant membranes overexpressing CSLD proteins that contained endogenous β-1,4-mannan activity and that the levels of β-mannan synthesis reported were significantly lower than those observed for GDP-Man-dependent mannan synthesis described for CSLA proteins (Liepman et al., 2005; Goubet et al., 2009). Both CSLD3 and CESA6 utilized UDP-Glc to synthesize β-1,4-glucan and did not appear to require the presence of either cellobiose or sitosterol-glucose primers (Lai-Kee-Him et al., 2002; Peng et al., 2002), similar to in vitro reconstituted CESA activities recently described for both bacteria (Omadjela et al., 2013) and plants (Purushotham et al., 2016; Cho et al., 2017). In vivo, CESA activities are thought to require assembly of hetero-oligomeric complexes with at least three distinct plant CESAs (Taylor et al., 2003; Somerville, 2006; Desprez et al., 2007; Persson et al., 2007). However, consistent with earlier in vitro reconstitution studies with purified hybrid aspen PttCESA8 or moss (*P. patens*) PpCESA8 (Purushotham et al., 2016; Cho et al., 2017), we observed accumulation of β-1,4-glucan in membranes containing only CESA6 proteins, suggesting that at least in vitro activities may not require assembly of hetero-oligomers. It should be noted, however, that the specific activity we report in reconstituted CESA6 proteoliposomes is significantly lower than those reported in vivo (Reiss et al., 1984).

In Arabidopsis, CSLD cell wall synthases are required for cell wall deposition during tip growth in root hairs and pollen tubes as well as for *de novo* cell wall deposition in newly forming cell plates in dividing cells (Favery et al., 2001; Wang et al., 2001; Bernal et al., 2008; Gu et al., 2016; Yang et al., 2016). While cellulose-specific stains have recently been used to show the presence of cellulose-like polysaccharides in growing root hairs and in newly forming cell plates during cytokinesis (Park et al., 2011; Miart et al., 2014), callose is likely the major cell wall component in these walls. At least during the early stages of deposition, characteristic arrays of cellulose microfibrils are not regularly observed in root hairs, pollen tubes, and forming cell plates (Meikle et al., 1991; Samuels et al., 1995; Ferguson et al., 1998; Chen and Kim, 2009; Drakakaki, 2015). Therefore, a major question is what kinds of β-1,4-glucan polymers do CSLD proteins synthesize? Based on size exclusion chromatography, we observed that detergent-solubilized protein complexes of both CSLD3 and CESA6 were organized into higher-order complexes of similar molecular size (Figure 7A), and ultrastructural analysis of these complexes by transmission electron microscopy revealed that both CSLD3 and CESA6 were present in particles of ~10- to 12-nm diameter with an apparent threefold symmetry (Figure 7C). Both the overall size and threefold symmetry are remarkably similar to proposed trimeric structures described for individual lobes of rosette terminal complexes from *P. patens* (Nixon et al., 2016) and trimeric complexes observed for recombinantly expressed and purified CESA1 catalytic domains (Vandavasi et al., 2016).

Why might land plants have evolved two distinct families of β-1,4-glucan synthases that can assemble into higher-order complexes? One of the distinguishing features of cellulose deposition in plant lineages is the organization of cellulose into paracrystalline microfibrils, whose deposition is associated with the orientation of an underlying array of cortical microtubules (Ledbetter and Porter, 1963). Indeed, the delivery (Crowell et al., 2009; Gutierrez et al., 2009), and migration upon cortical microtubules (Paredez et al., 2006; Desprez et al., 2007) appear to be intimately regulated by association of plasma membrane CSCs with a number of microtubule-associated proteins (Bringmann et al., 2012; Li et al., 2012; Lei et al., 2013; Liu et al., 2016). Earlier analysis of the CESA and CSLD gene families revealed that the CSLD genes display more diversity in their intron/exon organization, perhaps indicating that these are the older evolutionary group (Richmond and Somerville, 2001; Hazen et al., 2002; Little et al., 2018). Consistent with this, CSLD gene families are generally larger and more diverse in green algae, such as *Coleochaete orbicularis*, and bryophytes, including the moss *P. patens*, and the

vascular seedless plant *Selaginella moellendorffii* (Harholt et al., 2012; Mikkelsen et al., 2014). CSLDs are essential for the protonemal tip growth that occurs during vegetative growth in *P. patens* (Roberts and Bushoven, 2007). CSLD-dependent cell wall deposition appears to be essential in the apical plasma membranes of tip-growing cells (Doblin et al., 2001; Favery et al., 2001; Wang et al., 2001; Park et al., 2011) and during cell plate deposition in dividing cells (Gu et al., 2016; Yang et al., 2016): two cellular contexts in which plasma-membrane-associated cortical microtubules are generally absent (Emons and Ketelaar, 2012). One possibility is that CSLD complexes represent ancestral CSCs that synthesize cellulose microfibrils, but in a manner not as tightly associated with cortical microtubule organization. Evidence for a distinct, randomly distributed fibrillar cell wall element has been described in the apical domain of tip-growing root hairs (Newcomb and Bonnett, 1965; Akkerman et al., 2012; Emons and Ketelaar, 2012). Alternatively, while CESA-containing CSCs assemble into larger six-lobed rosette-like complexes, the CSLD-containing complexes we have observed (Figure 7C) may not. A major unresolved question is whether these CSLD3-containing particles assemble into similar rosette complex configurations in vivo, as with CESA-containing complexes, and whether the β-1,4-glucan polymers synthesized by these oligomeric CSLD complexes assemble into cellulose microfibrils that are similar or distinct in nature to those generated by CSCs containing CESA proteins.

METHODS

Plant Material and Growth Conditions

Arabidopsis (*Arabidopsis thaliana*) lines used in this study were derived from *Col-0* ecotype. The pCESA6::eYFP-CESA6-expressing line was kindly provided by Chris Somerville, University of California Berkeley (Paredez et al., 2006). Seeds were sterilized with 10% (v/v) Clorox bleach solution, rinsed five times with distilled water, then stored at 4°C for 2 d before being plated on growth medium comprised of 0.25× Murashige and Skoog (MS) basal medium,1% (w/v) Suc, and 0.6% (w/v) phytagel. Plates were placed vertically in a growth chamber at 21°C and grown under long-day conditions (16-h light [200 microEinstein/m^2s]/8-h dark photoperiod). For dark-grown conditions, plates were wrapped in aluminum foil. Three-day-old dark-grown seedlings were used for microscopy analysis. Five-day-old seedlings were used for morphology analysis. For propagation of mature plants, 14-d-old seedlings were transferred to soil and grown in environmental chambers at 21°C under long-day conditions (16-h light/8-h dark photoperiod).

Yeast Expression Plasmid Construction and Growth Conditions

Saccharomyces cerevisiae (strain INVSc1; Thermo Fisher Scientific, cat. no. C81000) was used for protein expression. Untransformed yeast was cultured in Yeast extract-Peptone-Dextrose medium. Positive colonies containing pYES2/NT C plasmids (Thermo Fisher Scientific, cat. no. V825220), expressing N-terminal His-tagged CESA6, CSLD3, or CSLA9 were selected and cultured overnight at 30°C and 180 rpm in SC-Ura + Glc medium composed of 1.9 g/L SC-Ura (uracil dropout) powder, 1.7 g/L yeast nitrogen base without amino acids and ammonium sulfate, 5 g/L ammonium sulfate, and 20 g/L Glc. Yeast cells were harvested, rinsed in sterile water, and used to inoculate 200 mL of SC-Ura + raffinose medium with the same nitrogenous base composition containing 20 g/L raffinose to an OD_{600} equal to 0.03. Cultures were grown for 14 to 16 h at 30°C and 180 rpm until the OD_{600} reached 2.0. Protein expression was induced by addition of 800 mL of SC-Ura + Gal medium containing 20 g/L Gal, and cells were incubated for an additional 6 h at 30°C and 180 rpm. Yeast cells were harvested, weighed, flash frozen in liquid nitrogen, and stored at −80°C.

Plant Expression Plasmid Construction and Plant Transformation

The CESA6 promoter was amplified (2251 bp upstream of ATG, primers shown in Supplemental Figure 8) and cloned into a pCAMBIA1301 vector upstream of a Citrine fluorescent protein coding sequence (Griesbeck et al., 2001), replacing the 35S promoter to generate pCambia1301:pCESA6. To construct the CESA6:D3CD chimeric protein coding sequence, the following three fragments were assembled: a CESA6 N-terminal domain fragment corresponding to CESA6 amino acids 1 to 321, a CSLD3 catalytic domain fragment corresponding to CSLD3 amino acids 340 to 921, and a CESA6 C-terminal fragment corresponding to CESA6 amino acids 861 to 1084. These three DNA fragments were ligated together and integrated into the pCambia1301:pCESA6 vector using the Gibson assembly method (Gibson et al., 2009). Point mutations for CESA6 (E463A, D464A) and the CESA6:D3CD chimera (corresponding to CSLD3 E508A and D509A) coding sequences were generated using PCR (shown in Supplemental Figure 8). Resulting N- and C-terminal fragments of the CESA6 and CESA6:D3CD chimera sequences were ligated together and integrated into the pCambia1301:pCESA6 vector by Gibson assembly. Plasmids were transformed into *Agrobacterium tumefaciens* strain GV3101 and then transferred to Arabidopsis using the standard floral-dip method (Clough and Bent, 1998).

Hypocotyl and Root Length Morphology Analysis

Images of 5-d-old seedlings were recorded using an Epson Perfection 4990 photo scanner. The lengths of hypocotyl and root regions were measured using Fiji-ImageJ (Schindelin et al., 2012). All transformed lines were grown side-by-side on the same plate, and at least 15 individuals were measured per line. Three independent biological replicates were performed for each line.

Cellulose Content

Ten-day-old dark-grown seedlings (with seed coats attached) were collected and rinsed five times with distilled water to remove Suc and residual MS medium. Samples were frozen in liquid nitrogen, ground to a fine powder, suspended in 80% (v/v) ethanol, filtered through a 45-μm nylon mesh (Industrial Netting, cat. no. WN0045), and then washed with 80% (v/v) ethanol followed by 100% ethanol. Cell wall residue was resuspended in a solution of chloroform:methanol (1:1) and shaken slowly for 2 h at room temperature. Cell wall residue was collected by filtration through a 45-μm nylon mesh and washed extensively with acetone, yielding alcohol insoluble residue for Updegraff analysis to determine cellulose content (Updegraff, 1969). In brief, 3 mL of acetic/nitric reagent was added to 2 mg of alcohol insoluble residue and boiled in a water bath for 30 min. Insoluble crystalline cellulose residue was collected by sedimentation in a Sorvall ST 16R centrifuge with TX-400 swinging bucket rotor at 5000 rpm for 5 min at room temperature., rinsed with 5 mL distilled water, resuspended in 1 mL of 67% (v/v) sulfuric acid, and incubated for 1 h at room temperature. Five milligrams of pure cellulose (Sigma-Aldrich, cat. no. C0806) was dried at 105°C for 6 h and dissolved in 1 mL of 67% (v/v) sulfuric acid, and then 50 mL distilled water was added to generate 100 μg/mL cellulose-sulfuric acid solution stock. The cellulose content was quantified by the anthrone assay with a standard curve containing 0, 4, 10, 20,

30 μg/mL cellulose-sulfuric acid solution diluted from the 100 μg/mL cellulose-sulfuric acid solution stock.

Fluorescent Imaging, Fluorescence Recovery After Photobleaching Analysis, and Colocalization Analysis

Images were acquired using a Leica confocal laser-scanning microscope SP8 using a 100× oil lens (Type F immersion oil, Numerical Aperture = 1.518) and processed with the Leica Application Suite X (LAS X) Life Science Microscope software. YFP and citrine fluorescence were excited at 514 nm and visualized from 519 nm to 650 nm. CSC particle movements were collected at 10-s intervals. Raw images were enlarged from 256*256 pixel images to 512*512 pixel images with Adobe Photoshop and imported into Fiji-ImageJ (Schindelin et al., 2012) to generate time projections using the Stacks function. CSC tracks were recorded using the segmented lines tool and analyzed by the Kymograph function in ImageJ. Particle velocities were calculated based on the distances measured in the kymograph over time. Photobleaching experiments (shown in Supplemental Figure 3) were performed by excitation of a Region Of Interest (red box) using a 405-nm laser, followed by collection of images at 10-s intervals. The red boxed region was cropped postcollection using Adobe Photoshop, and CSC particle numbers were analyzed using the Spot Counter function in ImageJ (box size, 3; noise tolerance, 30). For colocalization analysis, YFP/citrine and GFP fluorescence were excited at 488 nm and visualized from 524 nm to 650 nm, and 494 nm to 520 nm, respectively.

Yeast Protein Extraction, Purification, and Proteoliposome Reconstitution

Five grams of yeast cells (corresponding to 8 L of SC-Ura + Gal medium) expressing His-tagged CESA6, CSLD3, CSLA9, or an empty vector were resuspended in 20 mL lysis buffer (50 mM Hepes, pH 7.4, 300 mM NaCl, 1 mM $MgCl_2$, 1 mM $MnCl_2$, 5 mM cellobiose, 5% [v/v] glycerol, 50 mM Pefabloc SC plus [Sigma-Aldrich, cat. no. 11873601001], and 1 mM phenylmethylsulfonyl fluoride [Thermo Fisher Scientific, cat. no. 36,978]). Cells were lysed by passage through a French press (20,000 psi) twice at 4°C. Postnuclear supernatant was isolated by spinning in a SORVALL SS-34 rotor at 10,000 × *g* for 20 min at 4°C. A total membrane pellet was isolated by spinning the postnuclear supernatant fraction at 100,000 × *g* in a Fiberlite F65L-6 X 13.5 rotor at 4°C for 1 h. The supernatant was discarded, and the total membrane pellet was gently resuspended in 5 mL resuspension buffer (50 mM Hepes, pH 7.4, 300 mM NaCl, 1 mM $MgCl_2$, 1 mM $MnCl_2$, 5 mM cellobiose, 50 mM Pefabloc SC plus, 1 mM phenylmethylsulfonyl fluoride, and 2% [w/v] LFCE-14 [Anatrace, cat. no. L414]) and incubated at 4°C for 30 min with gentle end-over-end shaking. Resuspended membranes were then spun at 100,000 × *g* in a Fiberlite F65L-6 X 13.5 rotor at 4°C for 1 h, and the supernatant was carefully collected and incubated at room temperature with Ni-NTA slurry (Thermo Fisher Scientific, cat. no. 88,221) for 1 h. The slurry was transferred to a disposable chromatography column (Bio-Rad, cat. no. 7,321,010) and washed with 5 mL wash buffer (50 mM Hepes, pH 7.4, 300 mM NaCl, 1 mM $MgCl_2$, 1 mM $MnCl_2$, 5 mM cellobiose, 0.05% [w/v] LFCE-14, and 30 mM imidazole). Protein fractions (2.5 mL) were eluted from the Ni-NTA column with a 10-mL linear gradient of 30 to 250 mM imidazole in wash buffer. Protein fractions containing the His-tagged cell wall synthase enzymes were concentrated into wash buffer lacking imidazole using an Amicon Ultra 15 ultracel 100k centrifugal filter units (Sigma-Aldrich, cat. no. UFC910024) at 4000 × *g* for 10 min. For reconstitution of purified cell wall synthases into proteoliposomes, 10 mg of yeast lipids (Avanti, cat. no. 190000P) were dissolved in 1 mL chloroform in a glass test tube and then evaporated with nitrogen and dried in a vacuum chamber at room temperature for 1 h. The resulting yeast lipid film was resuspended in reconstruction buffer (50 mM Hepes, pH 7.4, 300 mM NaCl, 1 mM $MgCl_2$, 1 mM $MnCl_2$, 5 mM cellobiose, 6% [w/v] LFCE-14) and mixed with vigorous vortexing. Purified, detergent-solubilized proteins were mixed with 300 μL of the solubilized lipid fraction in a protein-to-lipid molar ratio of 1:4000 and incubated for 1 h at 4°C with gentle end-over-end shaking. Meanwhile, 0.2 g SM2 adsorbent beads (Bio-Rad, cat. no. 1,528,920) were washed with 1 mL bead buffer (50 mM, Hepes pH 7.4, 300 mM NaCl, 1 mM $MgCl_2$, 1 mM $MnCl_2$, 5 mM cellobiose) for 1 h at 4°C with gentle end-over-end shaking. The 300-μL protein-lipid mixture was diluted with 600 μL bead buffer and incubated with 0.2 g of prewashed SM2 adsorbent beads for 1 h. An additional 900 μL of bead buffer was added to the protein-lipid mixture, and the resulting 1800 μL protein-lipid mixture was transferred to a new tube containing 0.2 g of pre-washed SM2 adsorbent beads and incubated for 1 h with gentle end-over-end rotation. This step was repeated twice more (or a total of four SM2 adsorbent bead extractions) to completely extract the detergent. The resulting proteoliposomes were layered over a discontinuous Suc gradient (200 μL of 10%, 500 μL of each 15, 25, 35, and 60% [w/v] Suc in bead buffer) and spun for 2 h in a TH-660 swinging bucket rotor at 150,000 × *g* at 4°C. The proteoliposome layer (Supplemental Figure 5D, fraction 6) was collected and transferred to an Avanti Mini Extruder equipped with a 200-nm pore filter (cat. no. 610020) and passed through 20 to 30 times to generate unilamellar proteoliposomes of similar size, and then spun for 1 h in a Thermo Fisher Scientific TH-660 swinging bucket rotor at 150,000 × *g* at 4°C and resuspended with 100~200 μL bead buffer for UDP-Glo or GDP-Glo glycosyltransferase assays (Promega, cat. no. V6961, VA1090). In brief, 500- to 1000-ng proteoliposomes were incubated with 1 mM UDP-Glc in a 20-μL reaction containing 50 mM Hepes, pH 7.4, 300 mM NaCl, 1 mM $MgCl_2$, 1 mM $MnCl_2$, and 5 mM cellobiose for 1 h. Twenty microliters of freshly prepared nucleotide detection reagent was added and incubated for 15 min. Total luminescence was measured using a Tecan plate reader (infinite 200Pro; serial no. 1501003733), and the amount of UDP produced was calculated based on a UDP standard curve. For in vitro radiolabeling experiments with UDP-[^{3}H]-Glc, proteoliposomes equivalent to 1 to 2 μg of purified plant cell wall synthases were incubated with 0.25 μCi UDP-[^{3}H]-Glc (ARC, cat. no. ART 0127), 5 mM UDP-Glc in a 20-μL reaction containing 20 mM Tris (pH 7.5), 100 mM NaCl, 20 mM $MgCl_2$, 20 mM $MnCl_2$, 5 mM cellobiose, and 10% (v/v) glycerol at 37°C for 2 h. 0.1% Triton X-100 was added for reaction termination. Water-insoluble polymer was isolated by sedimentation in an Eppendorf 5415D centrifuge at 16,000 × *g* for 20 min at room temperature. The pellet was gently resuspended and incubated in 20 μL of 50 mM sodium acetate (pH 4.5), 100 mM NaCl, and 0.1 mg/mL of either endo-1,4-β-D-glucanase (Megazyme, cat. no. E-CELTR), or endo-1,3-β-D-glucanase (Megazyme, cat. no. E-LAMSE) at 37°C for 1 h. The pellet was collected by centrifuging at 16,000 × *g* for 20 min at room temperature and quantified by scintillation counting.

Size Exclusion Chromatography and Immunoblot Analysis

Three milligrams of purified, detergent-solubilized His-CSLD3, His-CESA6, and His-CSLA9 proteins in 5 mL wash buffer (50 mM Hepes, pH 7.4, 300 mM NaCl, 1 mM $MgCl_2$, 1 mM $MnCl_2$, 5 mM cellobiose, 0.05% [w/v] LFCE-14), were injected onto a HiPrep Sephacryl S-300 HR column equilibrated with wash buffer and run at a continuous flow rate of 0.5 mL/min. Two-milliliter fractions were collected starting at 30 mL, concentrated using Ultra 15 ultracel 100k centrifugal filter units, and every second fraction was analyzed by SDS-PAGE followed by either Coomassie Blue staining or immunoblotting. For immunoblotting, proteins were transferred to nitrocellulose membrane (GE Healthcare, cat. no. 10,600,003) by wet transfer at 15 V overnight. Membranes were blocked with 5% (w/v) skim milk in Phosphate-Buffered Saline containing 0.05% (v/v) Tween-20 (PBST). Membranes were then incubated with primary (Invitrogen, cat. no. MA1-21315, lot no. NI176305) and secondary (Thermo Fisher Scientific, cat. no. 31430, lot no. UB278606) antibodies at a 1:2000 dilution, respectively, washing 5× with PBST between steps. Horseradish peroxidase

chemiluminescence signal was then detected by x-ray film (Thermo Fisher Scientific, cat. no. 34,090) exposure.

Transmission Electron Microscopy

Following size-exclusion chromatography fractionation, protein samples were concentrated to ~500 μg/mL and applied to glow-discharged C-Flat holey carbon grids (Quantifoil R 1.2/1.3 Holey Carbon Films, Electron Microscopy Sciences, cat. no. Q250-CR1.3), incubated for 1 min, and negatively stained with 10 serial drops of 0.75% (w/v) uranyl formate. Samples were placed in a Technai T12 TEM operated at 120 keV, spherical aberration 2.0 mm (Cs), 50k magnification, and imaged with a 4k × 4k Gatan, Rio CMOS camera (Gatan).

Computational Model Building

The catalytic domain of RsBCSA (PDB ID: 5EIY; Morgan et al., 2016), residue indices 13 to 740 in UniProt sequence Q3J125), was extracted for our model. Structures for CSLD3, CESA6, and CSLA9 were constructed via homology modeling with PDB ID: 5EIY using the SWISS-MODEL webserver (Guex et al., 2009; Benkert et al., 2011; Bertoni et al., 2017; Bienert et al., 2017; Waterhouse et al., 2018). Protonation of titratable residues was performed at pH 7.2 using the H++ webserver (Anandakrishnan et al., 2012). Simulation-ready models were prepared using the Amber 16 software suite (Case et al., 2016). The models were solvated in explicit transferable intermolecular potential with 3 points (TIP3P) water molecules (Jorgensen et al., 1983) in a periodic box such that there were at least 10 Å of solvent on each side, and the protein was parameterized using the Amber ff14sb force field (Maier et al., 2015). The divalent cations in each enzyme's active site (Mg^{2+} in RsBCSA and Mn^{2+} in the plant enzymes) were parameterized using the Li/Merz parameters for TIP3P (Li et al., 2015), the product sugar chains used the GLYCAM06j force field (Kirschner et al., 2008), and the UDP-Glc and GDP-Man substrate parameters were taken from Petrová et al. [1999]. After solvation, chlorine ions were added to neutralize the overall system charge. Product sugar chains were added to each model based on homology to the position of the cellulose chain in the PDB ID: 5EIY crystal structure. The mannan chain was used in the CSLA9 structure by inversion of the chirality at the second carbon. Amino acid sequences from Arabidopsis CESA, CSLD, and CSLA family members were aligned by MUSCLE (Edgar, 2004) using MEGA 7 (Kumar et al., 2016).

Simulations and Energy Measurements

The initial coordinates for the UDP-Glc substrate in RsBCSA were taken directly from the PDB ID: 5EIY crystal structure. Each model was prepared for simulation in Amber 16 with 2500 steps of minimization followed by heating from 100 K to 300 K over 10,000 2-femtosec (fs) steps in a constant temperature and volume ensemble. Production simulations then followed in a constant temperature and pressure ensemble with a 2-fs timestep. The cutoff distance for nonbonded interactions was 8 Å, and the temperature was maintained at 300 K using the Andersen thermostat scheme with a randomization interval of 100 steps (Andersen, 1980). Covalent bonds to hydrogen atoms were restrained using the SHAKE algorithm (Ryckaert et al., 1977). Five parallel production simulations were performed for each combination of enzyme and substrate. First, 2-ns simulations were performed for BCSA, and the lowest energy conformations of each substrate were fitted into the homology models as initial coordinates for longer, 6-ns simulations, of which the first nanosecond was discarded from each for equilibration. Substrate binding energies were measured using the MMPBSA.py software (Miller et al., 2012) packaged in Amber 16. The solvent was stripped out from the models using the CPPTRAJ (Roe and Cheatham, 2013) and ParmEd software (https://github.com/ParmEd/ParmEd) packaged in Amber 16. The product chain in each model was included in the "protein" portion of the binding energy calculations (as opposed to the "ligand" portion), in order to isolate the binding energies of the nucleotide sugars alone.

Accession Numbers

Gene information in this article can be found in The Arabidopsis Information Resource database (https://www.arabidopsis.org) under the following accession numbers: AtCSLD3 (AT3G03050), AtCESA6 (AT5G64740), and AtCSLA9 (AT5G03760). Protein sequence data in this article can be found in the Uniprot Protein sequence database (https://www.uniprot.org/) under the following accession numbers: AtCSLD3 (Q9M9M4), AtCESA6 (Q94JQ6), AtCSLA9 (Q9LZR3), and RsBCSA (Q3J126, PDB ID: 5EIY).

Supplemental Data

Supplemental Figure 1. YFP and GFP signal can be distinguished using different emission spectrum ranges

Supplemental Figure 2. Inactive Citrine-CESA6-TAA and Citrine-CESA6:D3CD proteins are unable to rescue *cesa6* root elongation defects

Supplemental Figure 3. The fluorescence recovery rates of CSCs labeled with either Citrine-CESA6-TAA or Citrine-CESA6:D3CD-TAA after photobleaching

Supplemental Figure 4. Detergent solubilization of His-CSLD3, His-CESA6, and His-CSLD9 from yeast microsomal membranes

Supplemental Figure 5. Nickel affinity purification of LFCE-14 solubilized His-CSLD3, His-CESA6, and His-CSLD9

Supplemental Figure 6. UDP- and GDP-forming activities produced by His-CSLD3, His-CESA6, and His-CSLA9 are concentration and time dependent

Supplemental Figure 7. CSLDs are most closely related to CESA proteins

Supplemental Figure 8. Primers used for assembling CESA6:D3CD, CESA6-TAA, and CESA6:D3CD-TAA constructs

Supplemental Movie 1. Integration of EYFP-CESA6 into motile CSCs

Supplemental Movie 2. Integration of Citrine-CESA6:D3CD chimeric proteins into motile CSCs

Supplemental Movie 3. Catalytically dead Citrine-CESA6-TAA proteins integrate into CSCs with impaired motility characteristics

Supplemental Movie 4. Catalytically dead Citrine-CESA6:D3CD-TAA chimeric proteins integrate into immobile CSCs

Supplemental Movie 5. Molecular dynamics simulations of binding of UDP-glucose with BCSA, CESA6, and CSLD3 catalytic domains

Supplemental Movie 6. Molecular dynamics simulations of binding of UDP-glucose and GDP-mannose to the CSLA catalytic domain

Supplemental Movie 7. Molecular dynamics simulations of binding of GDP-mannose with BCSA, CESA6, and CSLD3 catalytic domains

ACKNOWLEDGMENTS

This article is based upon work supported by the National Science Foundation under grant no. 1817697. This work used the Extreme Science and Engineering Discovery Environment (XSEDE; Towns et al., 2014), which is supported by National Science Foundation grant no. ACI-1548562.

AUTHOR CONTRIBUTIONS

E.N., M.J.P, B.U., and H.B.M. conceived the study and designed the experiments; J.Y., G.B., T.B., and W.J.B. generated lines and constructs and performed the experiments; E.N., M.J.P, B.U., and H.B.M. analyzed the data; J.Y. and E.N. wrote the article. All authors revised the article.

Received August 19, 2019; revised February 11, 2020; accepted March 10, 2020; published March 13, 2020.

REFERENCES

Akkerman, M., Franssen-Verheijen, M.A., Immerzeel, P., Hollander, L.D., Schel, J.H., and Emons, A.M. (2012). Texture of cellulose microfibrils of root hair cell walls of *Arabidopsis thaliana*, *Medicago truncatula*, and *Vicia sativa*. J. Microsc. **247:** 60–67.

Anandakrishnan, R., Aguilar, B., and Onufriev, A.V. (2012). H++ 3.0: Automating pK prediction and the preparation of biomolecular structures for atomistic molecular modeling and simulations. Nucleic Acids Res. **40:** W537–W541.

Andersen, H.C. (1980). Molecular dynamics simulations at constant pressure and/or temperature. J. Chem. Phys. **72:** 2384–2393.

Arioli, T., et al. (1998). Molecular analysis of cellulose biosynthesis in *Arabidopsis*. Science **279:** 717–720.

Baskin, T.I. (2005). Anisotropic expansion of the plant cell wall. Annu. Rev. Cell Dev. Biol. **21:** 203–222.

Benkert, P., Biasini, M., and Schwede, T. (2011). Toward the estimation of the absolute quality of individual protein structure models. Bioinformatics **27:** 343–350.

Bernal, A.J., Jensen, J.K., Harholt, J., Sørensen, S., Moller, I., Blaukopf, C., Johansen, B., de Lotto, R., Pauly, M., Scheller, H.V., and Willats, W.G.T. (2007). Disruption of ATCSLD5 results in reduced growth, reduced xylan and homogalacturonan synthase activity and altered xylan occurrence in *Arabidopsis*. Plant J. **52:** 791–802.

Bernal, A.J., Yoo, C.M., Mutwil, M., Jensen, J.K., Hou, G., Blaukopf, C., Sørensen, I., Blancaflor, E.B., Scheller, H.V., and Willats, W.G.T. (2008). Functional analysis of the cellulose synthase-like genes CSLD1, CSLD2, and CSLD4 in tip-growing Arabidopsis cells. Plant Physiol. **148:** 1238–1253.

Bertoni, M., Kiefer, F., Biasini, M., Bordoli, L., and Schwede, T. (2017). Modeling protein quaternary structure of homo- and hetero-oligomers beyond binary interactions by homology. Sci. Rep. **7:** 10480.

Bienert, S., Waterhouse, A., de Beer, T.A., Tauriello, G., Studer, G., Bordoli, L., and Schwede, T. (2017). The SWISS-MODEL Repository: New features and functionality. Nucleic Acids Res. **45** (D1): D313–D319.

Boto, A.N., Xu, W., Jakoncic, J., Pannuri, A., Romeo, T., Bessman, M.J., Gabelli, S.B., and Amzel, L.M. (2011). Structural studies of the Nudix GDP-mannose hydrolase from *E. coli* reveals a new motif for mannose recognition. Proteins **79:** 2455–2466.

Bringmann, M., Li, E., Sampathkumar, A., Kocabek, T., Hauser, M.T., and Persson, S. (2012). POM-POM2/cellulose synthase interacting1 is essential for the functional association of cellulose synthase and microtubules in Arabidopsis. Plant Cell **24:** 163–177.

Burton, R.A., Wilson, S.M., Hrmova, M., Harvey, A.J., Shirley, N.J., Medhurst, A., Stone, B.A., Newbigin, E.J., Bacic, A., and Fincher, G.B. (2006). Cellulose synthase-like CslF genes mediate the synthesis of cell wall (1,3;1,4)-beta-D-glucans. Science **311:** 1940–1942.

Case, D.A., et al. (2016). AMBER 2016. (San Francisco: University of California, San Francisco).

Chebli, Y., Kaneda, M., Zerzour, R., and Geitmann, A. (2012). The cell wall of the Arabidopsis pollen tube: Spatial distribution, recycling, and network formation of polysaccharides. Plant Physiol. **160:** 1940–1955.

Chen, X.Y., and Kim, J.Y. (2009). Callose synthesis in higher plants. Plant Signal. Behav. **4:** 489–492.

Cho, S.H., Purushotham, P., Fang, C., Maranas, C., Díaz-Moreno, S.M., Bulone, V., Zimmer, J., Kumar, M., and Nixon, B.T. (2017). Synthesis and self-assembly of cellulose microfibrils from reconstituted cellulose synthase. Plant Physiol. **175:** 146–156.

Clough, S.J., and Bent, A.F. (1998). Floral dip: A simplified method for *Agrobacterium*-mediated transformation of *Arabidopsis thaliana*. Plant J. **16:** 735–743.

Cocuron, J.C., Lerouxel, O., Drakakaki, G., Alonso, A.P., Liepman, A.H., Keegstra, K., Raikhel, N., and Wilkerson, C.G. (2007). A gene from the cellulose synthase-like C family encodes a beta-1,4 glucan synthase. Proc. Natl. Acad. Sci. USA **104:** 8550–8555.

Cosgrove, D.J. (2005). Growth of the plant cell wall. Nat. Rev. Mol. Cell Biol. **6:** 850–861.

Cosgrove, D.J. (2018). Nanoscale structure, mechanics and growth of epidermal cell walls. Curr. Opin. Plant Biol. **46:** 77–86.

Crowell, E.F., Bischoff, V., Desprez, T., Rolland, A., Stierhof, Y.D., Schumacher, K., Gonneau, M., Höfte, H., and Vernhettes, S. (2009). Pausing of Golgi bodies on microtubules regulates secretion of cellulose synthase complexes in Arabidopsis. Plant Cell **21:** 1141–1154.

DeBolt, S., Gutierrez, R., Ehrhardt, D.W., Melo, C.V., Ross, L., Cutler, S.R., Somerville, C., and Bonetta, D. (2007). Morlin, an inhibitor of cortical microtubule dynamics and cellulose synthase movement. Proc. Natl. Acad. Sci. USA **104:** 5854–5859.

Desprez, T., Juraniec, M., Crowell, E.F., Jouy, H., Pochylova, Z., Parcy, F., Höfte, H., Gonneau, M., and Vernhettes, S. (2007). Organization of cellulose synthase complexes involved in primary cell wall synthesis in *Arabidopsis thaliana*. Proc. Natl. Acad. Sci. USA **104:** 15572–15577.

Dhugga, K.S., Barreiro, R., Whitten, B., Stecca, K., Hazebroek, J., Randhawa, G.S., Dolan, M., Kinney, A.J., Tomes, D., Nichols, S., and Anderson, P. (2004). Guar seed beta-mannan synthase is a member of the cellulose synthase super gene family. Science **303:** 363–366.

Doblin, M.S., De Melis, L., Newbigin, E., Bacic, A., and Read, S.M. (2001). Pollen tubes of *Nicotiana alata* express two genes from different beta-glucan synthase families. Plant Physiol. **125:** 2040–2052.

Doblin, M.S., Pettolino, F.A., Wilson, S.M., Campbell, R., Burton, R.A., Fincher, G.B., Newbigin, E., and Bacic, A. (2009). A barley cellulose synthase-like CSLH gene mediates (1,3;1,4)-beta-D-glucan synthesis in transgenic Arabidopsis. Proc. Natl. Acad. Sci. USA **106:** 5996–6001.

Drakakaki, G. (2015). Polysaccharide deposition during cytokinesis: Challenges and future perspectives. Plant Sci. **236:** 177–184.

Dwivany, F.M., Yulia, D., Burton, R.A., Shirley, N.J., Wilson, S.M., Fincher, G.B., Bacic, A., Newbigin, E., and Doblin, M.S. (2009). The CELLULOSE-SYNTHASE LIKE C (CSLC) family of barley includes members that are integral membrane proteins targeted to the plasma membrane. Mol. Plant **2:** 1025–1039.

Edgar, R.C. (2004). MUSCLE: Multiple sequence alignment with high accuracy and high throughput. Nucleic Acids Res. **32:** 1792–1797.

Emons, A.M.C., and Ketelaar, T. (2012). Root Hairs. (Berlin: Springer).

Fagard, M., Desnos, T., Desprez, T., Goubet, F., Refregier, G., Mouille, G., McCann, M., Rayon, C., Vernhettes, S., and Höfte, H. (2000). PROCUSTE1 encodes a cellulose synthase required for

normal cell elongation specifically in roots and dark-grown hypocotyls of Arabidopsis. Plant Cell **12:** 2409–2424.

Favery, B., Ryan, E., Foreman, J., Linstead, P., Boudonck, K., Steer, M., Shaw, P., and Dolan, L. (2001). KOJAK encodes a cellulose synthase-like protein required for root hair cell morphogenesis in *Arabidopsis*. Genes Dev. **15:** 79–89.

Ferguson, C., Teeri, T.T., Siika-aho, M., Read, S.M., and Bacic, A. (1998). Location of cellulose and callose in pollen tubes and grains of *Nicotiana tabacum*. Planta **206:** 452–460.

Galway, M.E., Eng, R.C., Schiefelbein, J.W., and Wasteneys, G.O. (2011). Root hair-specific disruption of cellulose and xyloglucan in AtCSLD3 mutants, and factors affecting the post-rupture resumption of mutant root hair growth. Planta **233:** 985–999.

Gibson, D.G., Young, L., Chuang, R.Y., Venter, J.C., Hutchison, C.A., III, and Smith, H.O. (2009). Enzymatic assembly of DNA molecules up to several hundred kilobases. Nat. Methods **6:** 343–345.

Goubet, F., Barton, C.J., Mortimer, J.C., Yu, X., Zhang, Z., Miles, G.P., Richens, J., Liepman, A.H., Seffen, K., and Dupree, P. (2009). Cell wall glucomannan in *Arabidopsis* is synthesised by CSLA glycosyltransferases, and influences the progression of embryogenesis. Plant J. **60:** 527–538.

Griesbeck, O., Baird, G.S., Campbell, R.E., Zacharias, D.A., and Tsien, R.Y. (2001). Reducing the environmental sensitivity of yellow fluorescent protein. Mechanism and applications. J. Biol. Chem. **276:** 29188–29194.

Gu, F., Bringmann, M., Combs, J.R., Yang, J., Bergmann, D.C., and Nielsen, E. (2016). Arabidopsis CSLD5 functions in cell plate formation in a cell cycle-dependent manner. Plant Cell **28:** 1722–1737.

Guex, N., Peitsch, M.C., and Schwede, T. (2009). Automated comparative protein structure modeling with SWISS-MODEL and Swiss-PdbViewer: A historical perspective. Electrophoresis **30** (Suppl 1): S162–S173.

Gutierrez, R., Lindeboom, J.J., Paredez, A.R., Emons, A.M.C., and Ehrhardt, D.W. (2009). *Arabidopsis* cortical microtubules position cellulose synthase delivery to the plasma membrane and interact with cellulose synthase trafficking compartments. Nat. Cell Biol. **11:** 797–806.

Harholt, J., Sørensen, I., Fangel, J., Roberts, A., Willats, W.G., Scheller, H.V., Petersen, B.L., Banks, J.A., and Ulvskov, P. (2012). The glycosyltransferase repertoire of the spikemoss *Selaginella moellendorffii* and a comparative study of its cell wall. PLoS One **7:** e35846.

Hazen, S.P., Scott-Craig, J.S., and Walton, J.D. (2002). Cellulose synthase-like genes of rice. Plant Physiol. **128:** 336–340.

Hu, H., Zhang, R., Tang, Y., Peng, C., Wu, L., Feng, S., Chen, P., Wang, Y., Du, X., and Peng, L. (2019). Cotton CSLD3 restores cell elongation and cell wall integrity mainly by enhancing primary cellulose production in the *Arabidopsis* cesa6 mutant. Plant Mol. Biol. **101:** 389–401.

Jorgensen, W.L., Chandrasekhar, J., Madura, J.D., Impey, R.W., and Klein, M.L. (1983). Comparison of simple potential functions for simulating liquid water. J. Chem. Phys. **79:** 926–935.

Kimura, S., Laosinchai, W., Itoh, T., Cui, X., Linder, C.R., and Brown, R.M., Jr. (1999). Immunogold labeling of rosette terminal cellulose-synthesizing complexes in the vascular plant vigna angularis. Plant Cell **11:** 2075–2086.

Kirschner, K.N., Yongye, A.B., Tschampel, S.M., González-Outeiriño, J., Daniels, C.R., Foley, B.L., and Woods, R.J. (2008). GLYCAM06: A generalizable biomolecular force field. Carbohydrates. J. Comput. Chem. **29:** 622–655.

Kumar, S., Stecher, G., and Tamura, K. (2016). MEGA7: Molecular evolutionary genetics analysis version 7.0 for bigger datasets. Mol. Biol. Evol. **33:** 1870–1874.

Lai-Kee-Him, J., Chanzy, H., Müller, M., Putaux, J.L., Imai, T., and Bulone, V. (2002). In vitro versus in vivo cellulose microfibrils from plant primary wall synthases: structural differences. J. Biol. Chem. **277:** 36931–36939.

Ledbetter, M.C., and Porter, K.R. (1963). A "microtubule" in plant cell fine structure. J. Cell Biol. **19:** 239–250.

Lei, L., Li, S., Du, J., Bashline, L., and Gu, Y. (2013). Cellulose synthase INTERACTIVE3 regulates cellulose biosynthesis in both a microtubule-dependent and microtubule-independent manner in Arabidopsis. Plant Cell **25:** 4912–4923.

Lei, L., Zhang, T., Strasser, R., Lee, C.M., Gonneau, M., Mach, L., Vernhettes, S., Kim, S.H., J Cosgrove, D., Li, S., and Gu, Y. (2014). The jiaoyao1 mutant is an allele of korrigan1 that abolishes endoglucanase activity and affects the organization of both cellulose microfibrils and microtubules in Arabidopsis. Plant Cell **26:** 2601–2616.

Lesage, G., and Bussey, H. (2006). Cell wall assembly in *Saccharomyces cerevisiae*. Microbiol. Mol. Biol. Rev. **70:** 317–343.

Li, P., Song, L.F., and Merz, K.M., Jr. (2015). Parameterization of highly charged metal ions using the 12-6-4 LJ-type nonbonded model in explicit water. J. Phys. Chem. B **119:** 883–895.

Li, S., Lei, L., Somerville, C.R., and Gu, Y. (2012). Cellulose synthase interactive protein 1 (CSI1) links microtubules and cellulose synthase complexes. Proc. Natl. Acad. Sci. USA **109:** 185–190.

Li, Y., Yang, T., Dai, D., Hu, Y., Guo, X., and Guo, H. (2017). Evolution, gene expression profiling and 3D modeling of CSLD proteins in cotton. BMC Plant Biol. **17:** 119.

Liepman, A.H., Wightman, R., Geshi, N., Turner, S.R., and Scheller, H.V. (2010). Arabidopsis: A powerful model system for plant cell wall research. Plant J. **61:** 1107–1121.

Liepman, A.H., Wilkerson, C.G., and Keegstra, K. (2005). Expression of cellulose synthase-like (Csl) genes in insect cells reveals that CslA family members encode mannan synthases. Proc. Natl. Acad. Sci. USA **102:** 2221–2226.

Little, A., Lahnstein, J., Jeffery, D.W., Khor, S.F., Schwerdt, J.G., Shirley, N.J., Hooi, M., Xing, X., Burton, R.A., and Bulone, V. (2019). A novel (1,4)-β-linked glucoxylan is synthesized by members of the *Cellulose Synthase-Like F* gene family in land plants. ACS Cent. Sci. **5:** 73–84.

Little, A., Schwerdt, J.G., Shirley, N.J., Khor, S.F., Neumann, K., O'Donovan, L.A., Lahnstein, J., Collins, H.M., Henderson, M., Fincher, G.B., and Burton, R.A. (2018). Revised phylogeny of the *Cellulose Synthase* gene superfamily: Insights into cell wall evolution. Plant Physiol. **177:** 1124–1141.

Liu, Z., Schneider, R., Kesten, C., Zhang, Y., Somssich, M., Zhang, Y., Fernie, A.R., and Persson, S. (2016). Cellulose-microtubule uncoupling proteins prevent lateral displacement of microtubules during cellulose synthesis in *Arabidopsis*. Dev. Cell **38:** 305–315.

Lombard, V., Golaconda Ramulu, H., Drula, E., Coutinho, P.M., and Henrissat, B. (2014). The carbohydrate-active enzymes database (CAZy) in 2013. Nucleic Acids Res. **42:** D490–D495.

MacKinnon, I.M., Sturcová, A., Sugimoto-Shirasu, K., His, I., McCann, M.C., and Jarvis, M.C. (2006). Cell-wall structure and anisotropy in procuste, a cellulose synthase mutant of *Arabidopsis thaliana*. Planta **224:** 438–448.

Maier, J.A., Martinez, C., Kasavajhala, K., Wickstrom, L., Hauser, K.E., and Simmerling, C. (2015). ff14SB: Improving the accuracy of protein side chain and backbone parameters from ff99SB. J. Chem. Theory Comput. **11:** 3696–3713.

Meikle, P.J., Bonig, I., Hoogenraad, N.J., Clarke, A.E., and Stone, B.A. (1991). The location of (1→3)-β-glucans in the walls of pollen tubes of *Nicotiana alata* using a (1→3)-β-glucan-specific monoclonal antibody. Planta **185:** 1–8.

Miart, F., Desprez, T., Biot, E., Morin, H., Belcram, K., Höfte, H., Gonneau, M., and Vernhettes, S. (2014). Spatio-temporal analysis of cellulose synthesis during cell plate formation in *Arabidopsis*. Plant J. **77:** 71–84.

Mikkelsen, M.D., Harholt, J., Ulvskov, P., Johansen, I.E., Fangel, J.U., Doblin, M.S., Bacic, A., and Willats, W.G. (2014). Evidence for land plant cell wall biosynthetic mechanisms in charophyte green algae. Ann. Bot. **114:** 1217–1236.

Miller, B.R., III, McGee, T.D., Jr., Swails, J.M., Homeyer, N., Gohlke, H., and Roitberg, A.E. (2012). MMPBSA.py: An efficient program for end-state free energy calculations. J. Chem. Theory Comput. **8:** 3314–3321.

Morgan, J.L.W., McNamara, J.T., Fischer, M., Rich, J., Chen, H.M., Withers, S.G., and Zimmer, J. (2016). Observing cellulose biosynthesis and membrane translocation in crystallo. Nature **531:** 329–334.

Morgan, J.L.W., Strumillo, J., and Zimmer, J. (2013). Crystallographic snapshot of cellulose synthesis and membrane translocation. Nature **493:** 181–186.

Newcomb, E.H., and Bonnett, H.T. (1965). Cytoplasmic microtubule and wall microfibril orientation in root hairs of radish. J. Cell Biol. **27:** 575–589.

Nixon, B.T., et al. (2016). Comparative structural and computational analysis supports eighteen cellulose synthases in the plant cellulose synthesis complex. Sci. Rep. 6: 28696.

Omadjela, O., Narahari, A., Strumillo, J., Mélida, H., Mazur, O., Bulone, V., and Zimmer, J. (2013). BcsA and BcsB form the catalytically active core of bacterial cellulose synthase sufficient for in vitro cellulose synthesis. Proc. Natl. Acad. Sci. USA **110:** 17856–17861.

Paredez, A.R., Somerville, C.R., and Ehrhardt, D.W. (2006). Visualization of cellulose synthase demonstrates functional association with microtubules. Science **312:** 1491–1495.

Park, S., Szumlanski, A.L., Gu, F., Guo, F., and Nielsen, E. (2011). A role for CSLD3 during cell-wall synthesis in apical plasma membranes of tip-growing root-hair cells. Nat. Cell Biol. **13:** 973–980.

Petrová, P., Koca, J., and Imberty, A. (1999). Potential energy hypersurfaces of nucleotide sugars: Ab initio calculations, force-field parametrization, and exploration of the flexibility. J. Am. Chem. Soc. **121:** 5535–5547.

Peng, L., Kawagoe, Y., Hogan, P., and Delmer, D. (2002). Sitosterol-beta-glucoside as primer for cellulose synthesis in plants. Science **295:** 147–150.

Persson, S., Paredez, A., Carroll, A., Palsdottir, H., Doblin, M., Poindexter, P., Khitrov, N., Auer, M., and Somerville, C.R. (2007). Genetic evidence for three unique components in primary cell-wall cellulose synthase complexes in *Arabidopsis*. Proc. Natl. Acad. Sci. USA **104:** 15566–15571.

Polko, J.K., and Kieber, J.J. (2019). The Regulation of Cellulose Biosynthesis in Plants. Plant Cell **31:** 282–296.

Purushotham, P., Cho, S.H., Díaz-Moreno, S.M., Kumar, M., Nixon, B.T., Bulone, V., and Zimmer, J. (2016). A single heterologously expressed plant cellulose synthase isoform is sufficient for cellulose microfibril formation in vitro. Proc. Natl. Acad. Sci. USA **113:** 11360–11365.

Reiss, H.D., Schnepf, E., and Herth, W. (1984). The plasma membrane of the *Funaria caulonema* tip cell: Morphology and distribution of particle rosettes, and the kinetics of cellulose synthesis. Planta **160:** 428–435.

Richmond, T.A., and Somerville, C.R. (2000). The cellulose synthase superfamily. Plant Physiol. **124:** 495–498.

Richmond, T.A., and Somerville, C.R. (2001). Integrative approaches to determining Csl function. Plant Mol. Biol. **47:** 131–143.

Roberts, A.W., and Bushoven, J.T. (2007). The cellulose synthase (CESA) gene superfamily of the moss *Physcomitrella patens*. Plant Mol. Biol. **63:** 207–219.

Roe, D.R., and Cheatham, T.E., III (2013). PTRAJ and CPPTRAJ: Software for processing and analysis of molecular dynamics trajectory data. J. Chem. Theory Comput. **9:** 3084–3095.

Ryckaert, J.-P., Ciccotti, G., and Berendsen, H.J.C. (1977). Numerical integration of the cartesian equations of motion of a system with constraints: molecular dynamics of n-alkanes. J. Comput. Phys. **23:** 327–341.

Samuels, A.L., Giddings, T.H., Jr., and Staehelin, L.A. (1995). Cytokinesis in tobacco BY-2 and root tip cells: A new model of cell plate formation in higher plants. J. Cell Biol. **130:** 1345–1357.

Scavuzzo-Duggan, T.R., Chaves, A.M., Singh, A., Sethaphong, L., Slabaugh, E., Yingling, Y.G., Haigler, C.H., and Roberts, A.W. (2018). Cellulose synthase 'class specific regions' are intrinsically disordered and functionally undifferentiated. J. Integr. Plant Biol. **60:** 481–497.

Scheible, W.R., and Pauly, M. (2004). Glycosyltransferases and cell wall biosynthesis: Novel players and insights. Curr. Opin. Plant Biol. **7:** 285–295.

Schindelin, J., Arganda-Carreras, I., Frise, E., Kaynig, V., Longair, M., Pietzsch, T., Preibisch, S., Rueden, C., Saalfeld, S., Schmid, B., Tinevez, J.Y., and White, D.J., et al. (2012). Fiji: An open-source platform for biological-image analysis. Nat. Methods **9:** 676–682.

Sethaphong, L., Haigler, C.H., Kubicki, J.D., Zimmer, J., Bonetta, D., DeBolt, S., and Yingling, Y.G. (2013). Tertiary model of a plant cellulose synthase. Proc. Natl. Acad. Sci. USA **110:** 7512–7517.

Slabaugh, E., Davis, J.K., Haigler, C.H., Yingling, Y.G., and Zimmer, J. (2014). Cellulose synthases: New insights from crystallography and modeling. Trends Plant Sci. **19:** 99–106.

Smith, P.J., Wang, H.-T., York, W.S., Peña, M.J., and Urbanowicz, B.R. (2017). Designer biomass for next-generation biorefineries: Leveraging recent insights into xylan structure and biosynthesis. Biotechnol. Biofuels **10:** 286.

Somerville, C. (2006). Cellulose synthesis in higher plants. Annu. Rev. Cell Dev. Biol. **22:** 53–78.

Taylor, N.G., Howells, R.M., Huttly, A.K., Vickers, K., and Turner, S.R. (2003). Interactions among three distinct CesA proteins essential for cellulose synthesis. Proc. Natl. Acad. Sci. USA **100:** 1450–1455.

Towns, J.W., et al. (2014). XSEDE: Accelerating scientific discovery. Comput. Sci. Eng. **16:** 62–74.

UniProt Consortium (2019). UniProt: A worldwide hub of protein knowledge. Nucleic Acids Res. **47** (D1): D506–D515.

Updegraff, D.M. (1969). Semimicro determination of cellulose in biological materials. Anal. Biochem. **32:** 420–424.

Vain, T., Crowell, E.F., Timpano, H., Biot, E., Desprez, T., Mansoori, N., Trindade, L.M., Pagant, S., Robert, S., Höfte, H., Gonneau, M., and Vernhettes, S. (2014). The cellulase KORRIGAN is part of the cellulose synthase complex. Plant Physiol. **165:** 1521–1532.

Vandavasi, V.G., et al. (2016). A structural study of CESA1 catalytic domain of Arabidopsis cellulose synthesis complex: Evidence for CESA trimers. Plant Physiol. **170:** 123–135.

Vergara, C.E., and Carpita, N.C. (2001). beta-D-glycan synthases and the CesA gene family: Lessons to be learned from the mixed-linkage (1 -> 3),(1 -> 4)beta-D-glucan synthase. Plant Mol. Biol. **47:** 145–160.

Verhertbruggen, Y., Yin, L., Oikawa, A., and Scheller, H.V. (2011). Mannan synthase activity in the CSLD family. Plant Signal. Behav. **6:** 1620–1623.

Wang, X., Cnops, G., Vanderhaeghen, R., De Block, S., Van Montagu, M., and Van Lijsebettens, M. (2001). AtCSLD3, a cellulose synthase-like gene important for root hair growth in Arabidopsis. Plant Physiol. **126:** 575–586.

Watanabe, Y., Schneider, R., Barkwill, S., Gonzales-Vigil, E., Hill, J.L., Jr., Samuels, A.L., Persson, S., and Mansfield, S.D. (2018). Cellulose synthase complexes display distinct dynamic behaviors during xylem transdifferentiation. Proc. Natl. Acad. Sci. USA **115:** E6366–E6374.

Waterhouse, A., Bertoni, M., Bienert, S., Studer, G., Tauriello, G., Gumienny, R., Heer, F.T., de Beer, T.A.P., Rempfer, C., Bordoli, L., Lepore, R., and Schwede, T. (2018). SWISS-MODEL: Homology modelling of protein structures and complexes. Nucleic Acids Res. **46** (W1): W296–W303.

Yang, W., Schuster, C., Beahan, C.T., Charoensawan, V., Peaucelle, A., Bacic, A., Doblin, M.S., Wightman, R., and Meyerowitz, E.M. (2016). Regulation of meristem morphogenesis by cell wall synthases in *Arabidopsis*. Curr. Biol. **26:** 1404–1415.

Yin, L., Verhertbruggen, Y., Oikawa, A., Manisseri, C., Knierim, B., Prak, L., Jensen, J.K., Knox, J.P., Auer, M., Willats, W.G.T., and Scheller, H.V. (2011). The cooperative activities of CSLD2, CSLD3, and CSLD5 are required for normal *Arabidopsis* development. Mol. Plant **4:** 1024–1037.

Yoshikawa, T., Eiguchi, M., Hibara, K., Ito, J., and Nagato, Y. (2013). Rice slender leaf 1 gene encodes cellulose synthase-like D4 and is specifically expressed in M-phase cells to regulate cell proliferation. J. Exp. Bot. **64:** 2049–2061.